Marine and Petroleum Geology 156 (2023) 106452

Contents lists available at ScienceDirect

Marine and Petroleum Geology

journal homepage: www.elsevier.com/locate/marpetgeo

# Formation mechanism of organic-rich mixed sedimentary rocks in saline lacustrine basin, Permian Lucaogou Formation, Jimsar Sag, Junggar Basin, Northwest China

Wenren Zeng [a,b], Zhihuan Zhang [a,b,*], Boran Wang [a,b], Xuan Chen [c], Ruihui Zheng [a,b], Guobin Fu [c], Ying Jin [c]

[a] *State Key Laboratory of Petroleum Resources and Prospecting, China University of Petroleum (Beijing), Beijing 102249, China*
[b] *College of Geoscience, China University of Petroleum, Beijing 102249, China*
[c] *PetroChina Tuha Oilfield Company, Hami 839009, China*

A R T I C L E I N F O

*Keywords:*
Lucaogou formation
Mixed sedimentary rocks
Element geochemistry
Biomarker
Palaeoenvironment
Primary productivity
Formation mechanism

A B S T R A C T

The organic-rich mixed sedimentary rocks deposited in a saline lacustrine environment are widespread in the Lucaogou Formation ($P_2l$), Jimsar Sag, Junggar Basin. These rocks have complex lithology (mainly including mudstone, dolomitic mudstone and argillaceous dolomite) and significant changes in geochemical characteristics. Presently, the formation mechanism of organic-rich mixed sedimentary rocks in the $P_2l$ of the Jimsar Sag is obscure. To address these issues, the formation mechanism of mudstone, dolomitic mudstone and argillaceous dolomite is revealed by evaluating their sedimentary environment, primary productivity and sources of organic matter using organic petrology, organic geochemistry and inorganic geochemistry. The results show that the mixed sedimentary rocks of the $P_2l$ exhibit excellent hydrocarbon generation potential. The mixed sedimentary strata were mainly deposited in saline and suboxic to anoxic water column, and the main source of organic matter was aquatic organisms. During the changes from mudstone, dolomite mudstone to argillaceous dolomite deposition, the paleoclimatic condition varied from warm-humid to arid-hot with more frequent hydrothermal activity, which enhanced the salinity of the water column, leading to a higher proportion of halotolerant algae (cyanobacteria and green algae). The improvement in the paleoproductivity caused by volcanic activity was the most critical factor to promote the enrichment of organic matter in the mixed sedimentary rocks. In addition, the decomposition of algae and stratified water column were conducive to the formation of a stable and suboxic to anoxic bottom water environment, which improves the preservation conditions of organic matter, and also favored the organic matter enrichment in mixed sedimentary rocks. Therefore, the frequent changes in paleoclimatic conditions and periodic hydrothermal activity controlled the formation of different lithologies in the $P_2l$. High primary productivity and good preservation conditions promoted the accumulation of organic matter in these mixed sedimentary rocks.

## 1. Introduction

In recent years, oil and gas resources related to mixed sedimentary strata have been found in many petroliferous basins (Ding et al., 2013; Wu et al., 2016; Cao et al., 2016; Liu et al., 2018; Zhang et al., 2019b; Zhi et al., 2023). In particular, mixed sedimentation makes important contributions to the formation and accumulation of unconventional oil and gas resources, and plays an important role in the exploration and development process (Poeppelreiter and Aigner, 2003; Palermo et al., 2008; Li et al., 2015, 2021c; Zhang et al., 2019a). Mixed sedimentation of terrigenous clastic and carbonate rocks develop in both marine and terrestrial sedimentary environments (Mount, 1984). The marine sedimentary environment is one of the most developed sedimentary environments of mixed sediments, with a relatively high salinity of the water column and better developed carbonate rocks, while it is difficult to form mixed sediments in the continental sedimentary environment except for lacustrine settings (Dorsey and Kidwell, 1999; Dong et al., 2009; Ding et al., 2013; Zhang et al., 2019a). Compared with the mixed

* Corresponding author. State Key Laboratory of Petroleum Resources and Prospecting, China University of Petroleum (Beijing), Beijing 102249, China.
*E-mail address:* zhangzh3996@vip.163.com (Z. Zhang).

https://doi.org/10.1016/j.marpetgeo.2023.106452
Received 8 May 2023; Received in revised form 13 July 2023; Accepted 6 August 2023
Available online 12 August 2023

silica-carbonate sediments in shallow marine, few studies have been completed on lacustrine mixed sedimentary systems, especially in saline lacustrine environments.

Organic-rich mixed sedimentary rocks are widely distributed in many saline lacustrine basins in China, such as the Lucaogou Formation ($P_2l$) in the Jimsar Sag and Santanghu Basin (Zhang et al., 2019a; Ding et al., 2020; Liu et al., 2018; Pan et al., 2021), the Paleogene Shahejie Formation in the Bohai Bay Basin (Tang et al., 2019), and the Paleogene Xingouzui Formation in the Jianghan Basin (Li et al., 2021c). Abundant unconventional oil and gas resources have been recently discovered in mixed sedimentary strata of the Junggar, Santanghu, Bohaiwan and Jianghan basins (Gao et al., 2016, 2018; Zhang et al., 2018b; Su et al., 2019a; Li et al., 2015), which opened a new chapter in the exploration and development of unconventional oil and gas resources in mixed sedimentary strata formed in saline lacustrine basin. However, current research on lacustrine mixed sedimentary rocks primarily focuses on sedimentation and reservoir characteristics (Palermo et al., 2008; Feng et al., 2013). Further studies are needed on the formation mechanism of organic-rich mixed sedimentary rocks.

Previous studies have shown that the formation of organic-rich mixed sedimentary rocks is closely related to primary productivity, preservation conditions and paleoclimate conditions (Gao et al., 2016, 2018; Zhang et al., 2018b; Su et al., 2019b; Li et al., 2015). However, there are some differences in the formation mechanism of organic-rich source rocks in different basins, and the research on the formation mechanism of mixed sedimentary rocks with different lithologies is limited. Compared with the Bohai Bay, Jianghan and Santanghu basins, the organic-rich mixed rocks of the $P_2l$ in the Jimsar Sag have certain uniqueness and complexity, which are mainly composed of mudstone, dolomitic mudstone and argillaceous dolomite formed in the saline lacustrine environment, accompanied by volcanic and hydrothermal activity (Wu et al., 2016; Qiu et al., 2016; Zhang et al., 2019a; Meng et al., 2022). It has been confirmed that the enrichment of organic matter in source rocks of the $P_2l$ in the Jimsar Sag is closely related to volcanic activity, and volcanic ash can release a large number of trace elements that promote algae bloom and improve primary productivity

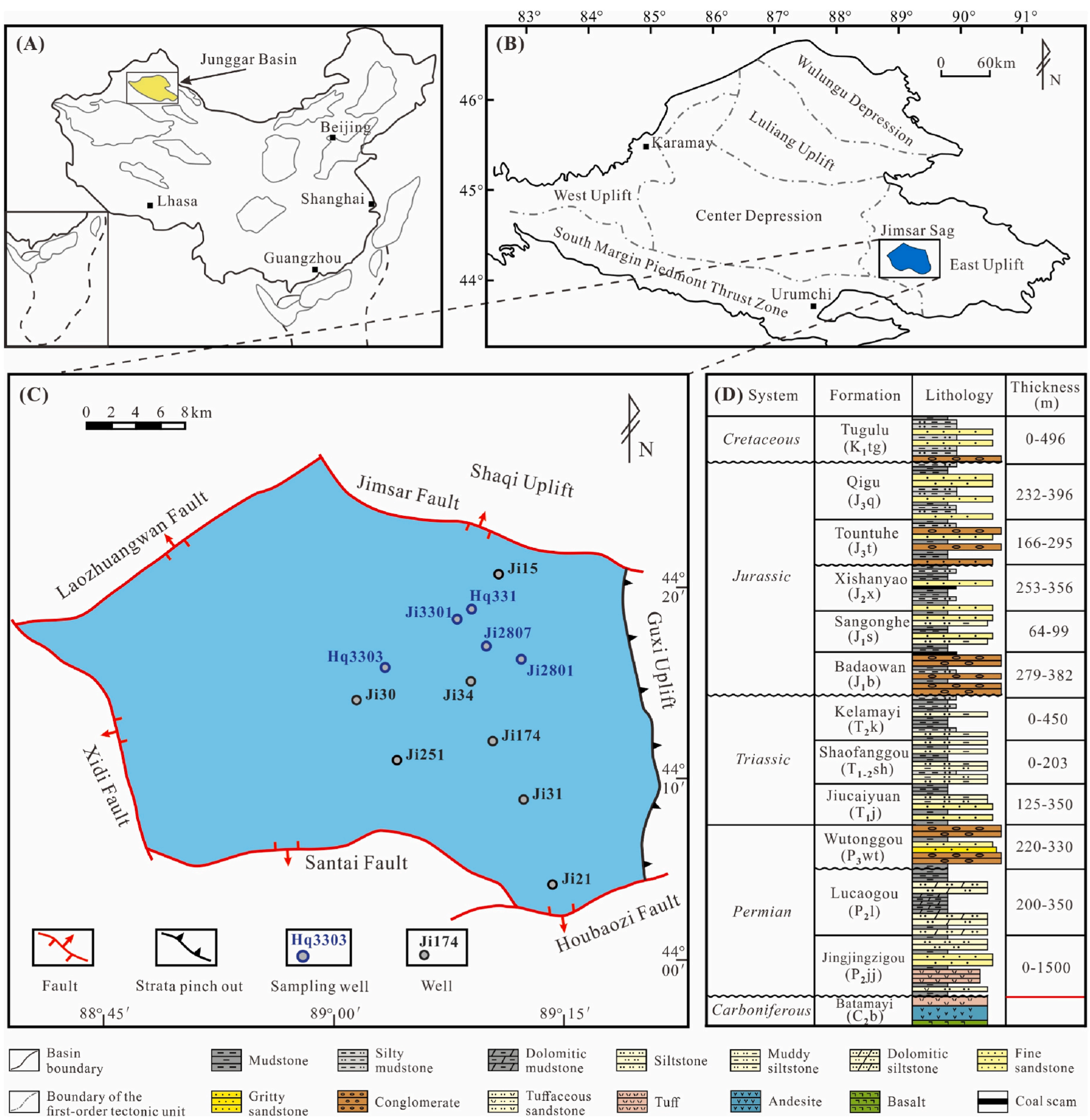


**Fig. 1.** Structure location map and stratigraphic column of the Jimsar Sag, Junggar Basin. (A) The Junggar basin located in northwestern China; (B) The Jimsar Sag located in the southeastern Junggar Basin; (C) Structural map of the Jimsar Sag, showing major faults, uplifts and key Wells; (D) Composite stratigraphic column in the Jimsar Sag (modified from Kuang et al., 2012; Wu et al., 2016; Liu et al., 2019).

(Ding et al., 2019; Kurenkov, 1966; Langmann et al., 2010; Hoffmann et al., 2012; Olgun et al., 2013). However, there are still some unresolved questions. For example, under the control of paleoclimate conditions, the effects of salinity on algae growth or algal population diversity in lacustrine basins are still unclear. In addition, most studies on organic matter enrichment of the $P_2l$ source rocks have regarded mudstone, dolomitic mudstone and argillaceous dolomite as a whole and ignored the differences in their formation mechanisms, which limits the prediction of high-quality source rock distribution areas.

In this work, organic geochemical, inorganic geochemical and organic petrological analyses of the samples were carried out to investigate the sedimentary environment and organic matter sources of the $P_2l$ mixed sedimentary rocks. The goal is to clarify the key factors controlling the formation of organic-rich mixed sedimentary rocks in the saline lake basin and to reveal the formation mechanism of different types of organic-rich mixed sedimentary rocks. The research results will provide a scientific basis for predicting the distribution of high-quality source rocks in the Permian, Jimsar Sag. Additionally, the findings of this study hold significant implications for understanding the formation mechanisms and predicting the development of high-quality source rocks in analogous saline lake basins.

## 2. Geological setting

The Junggar Basin, located in northwestern China, is an important part of the Central Asian Orogenic Belt (CAOB) (Fig. 1A and B) (Xiao et al., 2009). The Jimsar sag is a relatively independent dustpan-shaped depression located in the southwest of the eastern uplift belt of the Junggar Basin (Fig. 1B), surrounded by boundary faults and uplifts, with an area of about 1278 $km^2$ (Fig. 1C). The depression was initially formed at the end of the Late Paleozoic, and has experienced multi-stage tectonic movements such as Hercynian, Indosinian, Yanshan and Himalayan, which was filled by sedimentary strata from the Middle Permian to the Quaternary (Fig. 1D) (Fang et al., 2005, 2007).

The $P_2l$ is an important oil-bearing black fine grained rock series in the Jimsar Sag, with a stable thickness distribution of about 200–350 m (Fig. 1D). The $P_2l$ was deposited in saline lacustrine (Zhang et al., 2019a; Wang et al., 2021). The lithology of the $P_2l$ is relatively complex, consisting of a combination of terrigenous clastic and carbonate materials, accompanied by the input of volcanic materials (Qiu et al., 2016; Liu et al., 2019). The mudstone and carbonate rocks of the $P_2l$ have high hydrocarbon generation potential and are considered the main source rocks in the study area (Qiu et al., 2016; Cao et al., 2016; Gao et al., 2016).

## 3. Samples and methods

### 3.1. Samples

In this study, the selected samples were all representative core samples from wells in the Lucaogou Formation, exhibiting gray, gray-black or black. Each sample comprises an interval of about 0.5–2.0 m. In addition, the samples were collected from locations exhibiting significant changes in color and lithology, which are indicative of notable variations in the sedimentary environment of source rocks. 48 core samples of the $P_2l$ selected from 5 wells in the Jimsar Sag were systematically analyzed. The distribution of sampling Wells is shown in Fig. 1D. The samples include mudstone, dolomitic mudstone and argillaceous dolomite.

### 3.2. Methods

All source rock samples underwent total organic carbon (TOC), Rock-Eval pyrolysis analyses and X-ray diffraction (XRD). Representative source rock samples of different lithologies underwent organic petrographic analysis, solvent extraction, fractionation, gas chromatography-mass spectrometry (GC–MS) of saturated hydrocarbon, and elemental analysis. Elemental analysis was completed in the Analytical Laboratory of the Beijing Research Institute of Uranium Geology, China, and other experimental analysis were completed in the State Key Laboratory of Petroleum Resources and Prospecting at the China University of Petroleum (Beijing). The Chinese standard analyses used in this experiment are not fundamentally different from that of Western scholars.

#### 3.2.1. Mineral compositions analysis

The instrument was a Panalytical X 'Pert PRO X-ray diffractometer according to Chinese Oil and natural gas industry standard SY/T 5163-2018. Crushed samples (80-mesh) were mixed with ethanol, hand ground and then smear mounted on glass slides for X-ray diffraction analysis under the condition of temperature 24 °C and relative humidity 35%.

#### 3.2.2. TOC and Rock–Eval pyrolysis analyses

The TOC content was tested by the LECO CS-230 instrument according to Chinese National Standard GB/T19145-2022. The samples crushed to less than 80-mesh were pretreated with dilute hydrochloric acid (5%), rinsed with distilled water and dried in a drying oven for analysis. Rock-Eval pyrolysis analysis was carried out using a Rock-Eval 6 pyrolysis instrument according to Chinese National Standard GB/T18602-2016. During helium gas flow and gradual heating, pyrolytic materials (mg HC/g rock) were released from kerogen, and the free hydrocarbon content ($S_1$) and cracked hydrocarbon content ($S_2$) were successively tested at different temperatures. The temperature at which the second peak occurs corresponds to the maximum pyrolysis peak temperature ($T_{max}$).

#### 3.2.3. Organic petrographic analyses

Organic petrographic analyses mainly include maceral measurement and vitrinite reflectance (Ro) measurement. Maceral determination was performed using the Leica DM 4500P multipurpose microscope with random statistics of macerals along the vertical bedding direction under reflected white light and fluorescence. Maceral composition and classification in source rocks were determined according to ICCP System 1994 (ICCP, 1998, 2001) and Pickel et al. (2017). To ensure the accuracy of the results, at least 500 measurement points were randomly counted for each sample. Vitrinite reflectance (Ro) measurements are performed before calibration of the instrument using a standard sample (Ro = 0.904%), according to ISO 7404-5. To ensure the accuracy of the results, at least 50 measurement points were counted for each sample.

#### 3.2.4. Biomarker compounds analysis

Based on the organic matter extraction and separation, the saturated hydrocarbon samples obtained after separation were analyzed using an Agilent 6890 Gas Chromatograph (GC) equipped with the HP-5MS column (30-m × ) 0.25-mm i. d, with 0.25-μm film thickness) and linked with an Agilent 5975i Mass Spectrometer (MS). Helium was used as the carrier gas. The temperature range of the gradient heating mode was 50–310 °C, the temperature rise rate was 4 °C/min, and the test time for each sample was about 70 min. The ion source is electron ionization (EI). The scanning range of the detector is 50–550 M/z, and both scanning and simulation modes are used, and the Chinese National Standard GB/T 18606-2017 was used as a reference.

#### 3.2.5. Elemental analysis

The oxides of the major elements were measured on an Axios-mAX X-ray fluorescence (XRF) spectrometer and the Chinese National Standard GB/T 14506.28–2010 was used as a reference. The trace elements were analyzed using inductively coupled plasma mass spectrometry (ICP-MS) (NexION300D Plasma mass spectrometer) and were quantified based on Chines National Standard GB/T 14506.30–2010. Each ground sample was dissolved in a mixture of 30% HF and 68% $HNO_3$ in capped Teflon bombs at 150 °C for 48 h. The resultant solution was evaporated to near dryness again, followed by the addition of 1 mL of 6 M $HNO_3$. All samples were diluted for analysis, and the detection limits for the elements ranged from 0.1 ppb to 9 ppb. The precision and accuracy of the ICP-MS and X-ray fluorescence data are reported by Cullen et al. (2001), Qian et al. (2009), Wu et al. (2010) and Roser et al. (1995).

## 4. Results

### 4.1. Mineralogical characteristics

The lithology of the $P_2l$ in the Jimsar Sag changes frequently, and the lithology types of source rocks are mainly mudstone, dolomite mudstone and argillaceous dolomite (Qiu et al., 2016; Su et al., 2019b). The XRD analysis results show that the source rocks are mainly composed of plagioclase (6–61%, avg. 29.63%), dolomite (1–67%, avg. 27.15%), quartz (7–43%, avg. 21.88%) and clay minerals (1–59%, avg. 13.69%). The contents of potassium feldspar (0–14%, avg. 3.75%), calcite (0–15%, avg. 1.96%), analcite (0–13%, avg. 0.79%), pyrite (0–20%, avg. 0.69%) and siderite (0–8%, avg. 0.54%) are relatively low (Table 1). Among them, the content of dolomite (avg. 58.56%, avg. 33.50%, avg. 10.43%) in argillaceous dolomite, dolomitic mudstone and mudstone decreased successively, while the content of clay minerals (avg. 6.11%, avg. 11.44%, avg. 18.22%), quartz (avg. 12.44%, avg. 19.50%, avg. 27.22%) and plagioclase (avg. 18.78%, avg. 29.31%, avg. 34.09%) increased successively (Table 1).

### 4.2. Bulk geochemical parameters

In the study area, TOC and $S_1+S_2$ values of most samples are greater than 2% and 10.0 mg/g, respectively (Table 2), indicating that fine grained sediments of different lithologies in the $P_2l$ have abundant organic matter. As shown in the TOC and $S_1+S_2$ cross-plots, the source rock potential of these samples is mainly very good to excellent (Fig. 2A), and there is little difference in organic matter abundance between the source rocks of different lithologies. TOC values of mudstone, dolomite mudstone and argillaceous dolomite are

**Table 1**
XRD mineralogy data of samples from the Lucaogou Formation, Jimsar Sag.

| Sample | Well | Lithology | Depth (m) | 1 % | 2 % | 3 % | 4 % | 5 % | 6 % | 7 % | 8 % | 9 % |
|---|---|---|---|---|---|---|---|---|---|---|---|---|
| JL-1 | HQ3303 | A | 3832.12 | 16 | 30 | 0 | 42 | 0 | 12 | 0 | 0 | 0 |
| JL-2 | HQ3303 | A | 3833.16 | 3 | 34 | 0 | 61 | 0 | 2 | 0 | 0 | 0 |
| JL-3 | HQ3303 | A | 3833.83 | 2 | 32 | 12 | 42 | 0 | 4 | 8 | 0 | 0 |
| JL-4 | HQ3303 | A | 3834.70 | 2 | 25 | 11 | 47 | 6 | 10 | 2 | 0 | 0 |
| JL-5 | HQ3303 | A | 3835.72 | 7 | 22 | 10 | 44 | 11 | 3 | 3 | 0 | 0 |
| JL-6 | HQ3303 | A | 3836.45 | 1 | 28 | 14 | 43 | 0 | 8 | 6 | 0 | 0 |
| JL-7 | HQ3303 | A | 3840.42 | 3 | 28 | 14 | 36 | 8 | 6 | 5 | 0 | 0 |
| JL-8 | HQ3303 | A | 3845.42 | 12 | 34 | 0 | 47 | 0 | 4 | 0 | 3 | 0 |
| JL-9 | HQ3303 | A | 3972.30 | 13 | 43 | 0 | 28 | 0 | 16 | 0 | 0 | 0 |
| JL-10 | HQ3303 | A | 3975.54 | 2 | 31 | 7 | 40 | 0 | 20 | 0 | 0 | 0 |
| JL-11 | HQ331 | A | 3292.95 | 8 | 27 | 4 | 38 | 0 | 23 | 0 | 0 | 0 |
| JL-12 | J2801 | A | 2904.04 | 59 | 23 | 0 | 13 | 4 | 1 | 0 | 0 | 0 |
| JL-13 | J2801 | A | 2929.10 | 25 | 31 | 0 | 28 | 0 | 12 | 0 | 1 | 3 |
| JL-14 | J2801 | A | 3047.25 | 38 | 18 | 0 | 18 | 7 | 18 | 0 | 1 | 0 |
| JL-15 | J2801 | A | 3049.40 | 37 | 38 | 0 | 6 | 0 | 16 | 0 | 3 | 0 |
| JL-16 | J2801 | A | 3055.52 | 15 | 25 | 2 | 33 | 4 | 21 | 0 | 0 | 0 |
| JL-17 | J2802 | A | 2930.23 | 42 | 18 | 0 | 17 | 0 | 10 | 0 | 0 | 13 |
| JL-18 | J2807 | A | 3451.48 | 9 | 39 | 0 | 42 | 0 | 8 | 2 | 0 | 0 |
| JL-19 | J3301 | A | 3397.68 | 52 | 26 | 3 | 13 | 5 | 1 | 0 | 0 | 0 |
| JL-20 | J3301 | A | 3402.56 | 39 | 17 | 2 | 35 | 0 | 7 | 0 | 0 | 0 |
| JL-21 | J3301 | A | 3546.42 | 7 | 26 | 3 | 46 | 0 | 14 | 0 | 3 | 1 |
| JL-22 | J3301 | A | 3548.40 | 25 | 12 | 9 | 35 | 8 | 11 | 0 | 0 | 0 |
| JL-23 | J3301 | A | 3558.49 | 2 | 19 | 6 | 30 | 3 | 13 | 0 | 20 | 7 |
| JL-24 | HQ3303 | B | 3831.72 | 8 | 21 | 0 | 42 | 0 | 29 | 0 | 0 | 0 |
| JL-25 | HQ3303 | B | 3963.86 | 9 | 23 | 6 | 27 | 0 | 35 | 0 | 0 | 0 |
| JL-26 | HQ3303 | B | 3969.86 | 8 | 18 | 6 | 30 | 0 | 38 | 0 | 0 | 0 |
| JL-27 | HQ3303 | B | 3970.76 | 6 | 23 | 2 | 40 | 0 | 29 | 0 | 0 | 0 |
| JL-28 | HQ3303 | B | 3979.10 | 6 | 16 | 5 | 34 | 0 | 39 | 0 | 0 | 0 |
| JL-29 | HQ3303 | B | 3988.04 | 4 | 25 | 3 | 21 | 15 | 32 | 0 | 0 | 0 |
| JL-30 | HQ3303 | B | 3992.00 | 9 | 11 | 5 | 30 | 0 | 45 | 0 | 0 | 0 |
| JL-31 | J2801 | B | 2908.20 | 15 | 27 | 0 | 31 | 0 | 27 | 0 | 0 | 0 |
| JL-32 | J2801 | B | 2911.48 | 8 | 19 | 5 | 33 | 0 | 35 | 0 | 0 | 0 |
| JL-33 | J2801 | B | 2942.00 | 6 | 16 | 8 | 37 | 0 | 33 | 0 | 0 | 0 |
| JL-34 | J2801 | B | 3059.53 | 6 | 23 | 3 | 30 | 10 | 28 | 0 | 0 | 0 |
| JL-35 | J2801 | B | 3069.20 | 26 | 16 | 0 | 11 | 3 | 36 | 0 | 0 | 8 |
| JL-36 | J3301 | B | 3400.15 | 26 | 15 | 0 | 21 | 0 | 38 | 0 | 0 | 0 |
| JL-37 | J3301 | B | 3433.06 | 15 | 22 | 1 | 32 | 0 | 27 | 0 | 0 | 3 |
| JL-38 | J3301 | B | 3541.80 | 14 | 15 | 9 | 25 | 0 | 35 | 0 | 2 | 0 |
| JL-39 | J3301 | B | 3551.67 | 17 | 22 | 4 | 25 | 2 | 30 | 0 | 0 | 0 |
| JL-40 | HQ3303 | C | 3841.10 | 4 | 12 | 5 | 21 | 0 | 58 | 0 | 0 | 0 |
| JL-41 | HQ3303 | C | 3976.92 | 4 | 10 | 3 | 21 | 0 | 62 | 0 | 0 | 0 |
| JL-42 | HQ331 | C | 3295.60 | 4 | 17 | 0 | 20 | 0 | 59 | 0 | 0 | 0 |
| JL-43 | J2801 | C | 2929.94 | 14 | 7 | 5 | 15 | 0 | 56 | 0 | 0 | 3 |
| JL-44 | J2807 | C | 3453.16 | 4 | 9 | 3 | 18 | 0 | 66 | 0 | 0 | 0 |
| JL-45 | J3301 | C | 3399.12 | 13 | 22 | 0 | 12 | 2 | 51 | 0 | 0 | 0 |
| JL-46 | J3301 | C | 3542.16 | 4 | 10 | 1 | 18 | 0 | 67 | 0 | 0 | 0 |
| JL-47 | J3301 | C | 3547.72 | 2 | 13 | 6 | 19 | 6 | 54 | 0 | 0 | 0 |
| JL-48 | J3301 | C | 3554.42 | 6 | 12 | 3 | 25 | 0 | 54 | 0 | 0 | 0 |

Note: A. Mudstone; B. Dolomitic mudstone; C. Argillaceous dolomite; 1. Clay; 2. Quartz; 3. Potash feldspar; 4. Plagioclase; 5. Calcite; 6. Dolomite; 7. Siderite; 8. Pyrite; 9. Analcite.

**Table 2**
The TOC, Rock-Eval pyrolysis and organic maceral data of the samples from the Lucaogou Formation, Jimsar Sag.

| Sample | Lithology | 1 | 2 | 3 | 4 | 5 | 6 | 7 | 8 | 9 |
|---|---|---|---|---|---|---|---|---|---|---|
| JL-1 | A | 6.91 | 2.58 | 24.69 | 27.27 | 357.41 | 440 | 0.77 | 84.3 | 15.7 |
| JL-2 | A | 1.57 | 2.11 | 2.34 | 4.45 | 148.76 | 428 | – | – | – |
| JL-3 | A | 2.32 | 1.38 | 11.58 | 12.96 | 499.14 | 437 | – | – | – |
| JL-4 | A | 2.55 | 1.29 | 13.49 | 14.78 | 529.02 | 436 | – | – | – |
| JL-5 | A | 2.25 | 8.21 | 6.14 | 14.35 | 273.50 | 438 | – | – | – |
| JL-6 | A | 2.43 | 2.57 | 13.55 | 16.12 | 557.61 | 440 | – | – | – |
| JL-7 | A | 3.98 | 1.67 | 7.21 | 8.88 | 181.11 | 436 | – | – | – |
| JL-8 | A | 3.65 | 3.23 | 14.48 | 17.71 | 396.71 | 443 | 0.78 | 49.37 | 50.63 |
| JL-9 | A | 5.66 | 10.66 | 29.02 | 39.68 | 512.81 | 437 | 0.75 | 41.27 | 58.73 |
| JL-10 | A | 2.79 | 6.36 | 14.25 | 20.61 | 510.75 | 437 | – | – | – |
| JL-11 | A | 12.90 | 4.50 | 71.85 | 76.35 | 556.98 | 443 | 0.75 | 89.63 | 10.37 |
| JL-12 | A | 7.08 | 6.17 | 39.03 | 45.20 | 551.27 | 435 | 0.68 | 73.55 | 26.45 |
| JL-13 | A | 6.74 | 1.36 | 37.27 | 38.63 | 552.97 | 437 | – | – | – |
| JL-14 | A | 7.60 | 7.73 | 59.97 | 67.70 | 789.11 | 434 | – | – | – |
| JL-15 | A | 0.39 | 0.60 | 0.48 | 1.08 | 123.08 | 433 | – | – | – |
| JL-16 | A | 7.30 | 5.19 | 53.31 | 58.49 | 730.23 | 438 | – | – | – |
| JL-17 | A | 8.48 | 6.61 | 56.32 | 62.93 | 664.15 | 440 | 0.90 | 79.52 | 20.48 |
| JL-18 | A | 5.86 | 3.61 | 27.65 | 31.26 | 471.84 | 437 | – | – | – |
| JL-19 | A | 7.26 | 6.20 | 46.91 | 53.11 | 646.14 | 443 | 0.91 | 89.15 | 10.85 |
| JL-20 | A | 5.85 | 4.17 | 36.57 | 40.74 | 625.13 | 441 | – | – | – |
| JL-21 | A | 10.50 | 4.02 | 69.38 | 73.40 | 660.80 | 442 | – | – | – |
| JL-22 | A | 1.61 | 7.63 | 6.50 | 14.13 | 403.73 | 429 | – | – | – |
| JL-23 | A | 3.69 | 15.97 | 15.90 | 31.87 | 430.89 | 435 | – | – | – |
| JL-24 | B | 3.67 | 2.07 | 12.93 | 15.00 | 352.32 | 439 | 0.76 | 42.56 | 57.44 |
| JL-25 | B | 3.52 | 6.92 | 15.34 | 22.26 | 435.80 | 439 | – | – | – |
| JL-26 | B | 8.38 | 2.42 | 41.00 | 43.42 | 489.49 | 441 | 0.63 | 87.18 | 12.82 |
| JL-27 | B | 1.24 | 0.85 | 2.22 | 3.07 | 179.32 | 440 | – | – | – |
| JL-28 | B | 7.25 | 1.22 | 33.97 | 35.19 | 468.49 | 446 | 0.71 | 82.33 | 17.67 |
| JL-29 | B | 3.66 | 1.37 | 11.30 | 12.67 | 308.66 | 449 | – | – | – |
| JL-30 | B | 2.76 | 0.57 | 9.70 | 10.27 | 351.83 | 444 | – | – | – |
| JL-31 | B | 3.15 | 2.24 | 17.72 | 19.96 | 562.54 | 444 | – | – | – |
| JL-32 | B | 4.50 | 4.43 | 26.47 | 30.90 | 588.22 | 442 | 0.72 | 59.26 | 40.74 |
| JL-33 | B | 1.10 | 0.33 | 2.10 | 2.43 | 190.91 | 437 | – | – | – |
| JL-34 | B | 12.40 | 8.76 | 98.78 | 107.54 | 796.61 | 434 | – | – | – |
| JL-35 | B | 1.02 | 0.48 | 3.28 | 3.76 | 321.57 | 437 | – | – | – |
| JL-36 | B | 6.76 | 1.75 | 52.28 | 54.03 | 773.37 | 442 | – | – | – |
| JL-37 | B | 0.90 | 1.19 | 3.67 | 4.86 | 407.78 | 443 | – | – | – |
| JL-38 | B | 6.60 | 1.75 | 54.02 | 55.77 | 818.48 | 440 | 0.78 | 67.42 | 32.58 |
| JL-39 | B | 5.70 | 1.99 | 46.27 | 48.25 | 811.67 | 440 | 0.83 | 55.37 | 44.63 |
| JL-40 | C | 5.80 | 9.92 | 31.68 | 41.59 | 546.12 | 436 | 0.81 | 77.35 | 22.65 |
| JL-41 | C | 2.55 | 1.79 | 9.21 | 11.00 | 360.89 | 442 | – | – | – |
| JL-42 | C | 4.35 | 5.26 | 21.26 | 26.52 | 488.74 | 432 | 0.76 | 56.27 | 43.73 |
| JL-43 | C | 0.40 | 0.16 | 0.49 | 0.65 | 122.50 | 436 | – | – | – |
| JL-44 | C | 10.60 | 2.07 | 61.71 | 63.78 | 582.17 | 435 | 0.79 | 92.34 | 7.66 |
| JL-45 | C | 2.53 | 1.44 | 12.26 | 13.70 | 484.58 | 442 | – | – | – |
| JL-46 | C | 6.15 | 2.54 | 45.70 | 48.24 | 743.09 | 443 | 0.83 | 81.43 | 18.57 |
| JL-47 | C | 2.65 | 3.20 | 9.28 | 12.47 | 350.00 | 437 | – | – | – |
| JL-48 | C | 2.86 | 16.93 | 11.39 | 28.32 | 398.25 | 430 | – | – | – |

Note: A. Mudstone; B. Dolomitic mudstone; C. Argillaceous dolomite; 1. TOC = Total organic carbon (wt%); 2. $S_1$: Rock-Eval measured free hydrocarbons (mg HC/g rock); 3. $S_2$: Hydrocarbons generated during Rock Eval pyrolysis (mg HC/g rock); 4. PY: Generative potential = $S_1 + S_2$, (mg HC/g rock); 5. HI: Hydrogen index = ($S_2$/TOC) × 100, (mg HC/g TOC); 6. $T_{max}$ = Temperature maximum (°C); 7. Ro = Vitrinite reflectance (%); 8. Alginite: Alginite includes lamalginite and telalginite, vol%, mmf (Pickel et al., 2017); 9. Terrigenous: Terrigenous organic matter includes sporinite, vitrinite and inertinite, vol%, mmf (ICCP, 1998, 2001; Pickel et al., 2017).

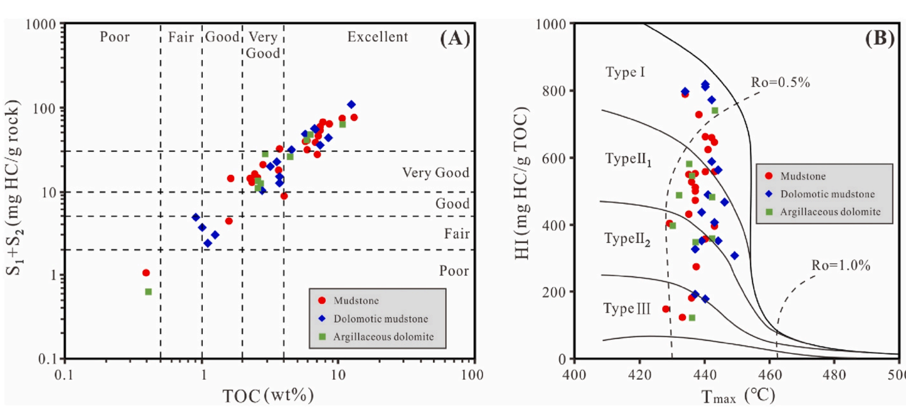


**Fig. 2.** (A) Plot of potential of generating hydrocarbon ($S_1$+$S_2$) vs. Total organic carbon (TOC) of source rock samples from the $P_2l$ (according to Peters and Cassa, 1994); (B) Plot of Hydrogen index (HI) vs. Temperature maximum ($T_{max}$) of source rock samples from the $P_2l$ (according to Peters and Cassa, 1994).

0.39–12.90 wt% (avg. 5.19 wt%), 0.90–12.40 wt% (avg. 4.54 wt%) and 0.40–10.60 wt% (avg. 4.21 wt%), respectively (Table 2). The $S_1+S_2$ values of mudstone, dolomite mudstone and argillaceous dolomite are 1.08–76.35 mg/g (avg. 33.55 mg/g), 2.43–107.54 mg/g (avg. 29.34 mg/g) and 0.65–63.78 mg/g (avg. 27.36 mg/g), respectively (Table 2).

The hydrogen index (HI) values of mudstone, dolomite mudstone and argillaceous dolomite are 123–789 mg HC/g TOC (avg. 486 mg HC/g TOC), 179–818 mg HC/g TOC (avg. 491 mg HC/g TOC) and 123–743 mg HC/g TOC (avg. 453 mg HC/g TOC), respectively (Table 2), reflecting that the hydrogen index (HI), which reflects the hydrocarbon generation potential and the type of organic matter of source rocks, is not significantly different among the different lithologies. As shown in HI and $T_{max}$ cross-plots, most source rocks are in the fields of type I-$II_1$ kerogen, and there is no significant difference among the source rock with different lithologies (Fig. 2B). In addition, the thermal evolution of source rocks is in the low mature to mature stage (Fig. 2B).

### 4.3. Organic petrology

Organic macerals in the $P_2$l of the study area are mainly derived from algae and terrigenous organic matter (Table 2). Therefore, to facilitate a better discussion on the source of organic matter, we have classified maceral components into two distinct categories: alginite (telalginite and lamalginite) representing the source of algae organic matter (Xie et al., 2014; Pickel et al., 2017), and terrestrial OM (sporinite, vitrinite and inertinite) representing a source of terrigenous higher plants organic matter (Bechtel et al., 2012; Xie et al., 2014).

The macerals in the source rocks are mainly composed of alginite (41.27–92.34 vol%, avg. 71.08 vol%), and the maceral content of terrigenous OM (mainly include sporinite, vitrinite and inertinite) is low to medium (7.66–58.73 vol%, avg. 28.92 vol%) (Table 2; Fig. 3). The maceral content of terrigenous OM in mudstone, dolomitic mudstone and argillaceous dolomite (10.85–58.73 vol%, avg. 27.60 vol%; 12.82–57.44 vol%, avg. 34.31 vol%; 7.66–43.73 vol%, avg. 23.15 vol%) is lower than that of alginite OM (41.27–89.62 vol%, avg. 72.40 vol%; 42.56–87.18 vol%, avg. 65.69 vol%; 56.27–92.34 vol%, avg. 76.85 vol %), and there is no significant difference in organic maceral composition of the source rocks with different lithologies.

The alginite in the source rocks of the $P_2$l are mainly composed of lamalginites, which are long strips and appear with strong green-yellow fluorescence (Fig. 3A and B). Some samples contain wavy anastomosing lamalginites, which were preserved to different degrees and display fold-overs (Fig. 3B), indicating a cohesive biofilm of extracellular polymeric substances, suggesting a cohesive microbial mat facies under incident blue light (Wingender et al., 1999). Telalginite was poorly preserved and present in low amounts (Fig. 3C).

The sporinite appears in a hollow, elongated, smooth-edged ring, with orange fluorescence (Fig. 3D). The inertinite appears at a relatively low content (Fig. 3E). The maceral from terrigenous OM is mainly composed of vitrinite, which appears as strip-shaped or irregularly shaped polygons (Fig. 3E and F). Under white light, the vitrinite is gray or dark gray (Fig. 3E and F). The measured $R_o$ of source rocks ranges from 0.63 to 0.91% (avg. 0.77%), reflecting that the thermal evolution of most source rocks is in the low mature to mature stage (Table 2).

### 4.4. Biomarkers

#### 4.4.1. Straight chain alkanes and isoprenoids

The N-alkanes in source rock samples of the $P_2$l are distributed in the range of $NC_{15}$ to $NC_{33}$, with a peak dominantly located at $NC_{17}$ to $NC_{23}$ (Fig. 4A and B), indicating that N-alkanes are dominated by short-chain N-alkanes. The carbon preference index (CPI) values range from 1.15 to 1.85 with an average of 1.41 (Table 4), indicating that there is no obvious odd-even predominance. The ratios of $\Sigma NC_{21-}/\Sigma NC_{22+}$ range from 0.69 to 1.85 (avg. 1.11) and the ratios of Pr/Ph range from 0.75 to 1.36 (avg. 1.04), with little difference among the source rocks with different lithologies (Table 4). There was no correlation between the Pr/Ph ratio and maturity parameters ($T_{max}$, *Ro*, 22S/(22S + 22R)$C_{31}$ Hopanes, 20S/(20S + 20R)$C_{29}$ Steranes and ββ/(αα+ββ)$C_{29}$ Steranes), which reflects that the effect of maturity on Pr/Ph ratio could be excluded.

#### 4.4.2. β–carotane

A high abundance of β-carotane was detected in the total ion chromatogram (TIC) of most source rock samples of the $P_2$l (Fig. 4A). The β-carotane index, β-carotane/17α 21β $C_{30}$ hopane, ranged from 0.15 to 1.91, with an average of 0.75 (Table 4). The mudstone, dolomite mudstone, and argillaceous dolomite are significantly different in β-carotane index, with an increased β-carotane index of 0.15–1.78 (avg. 0.56), 0.51 to 1.32 (avg. 0.83), and 0.69 to 1.91 (avg. 1.21), respectively

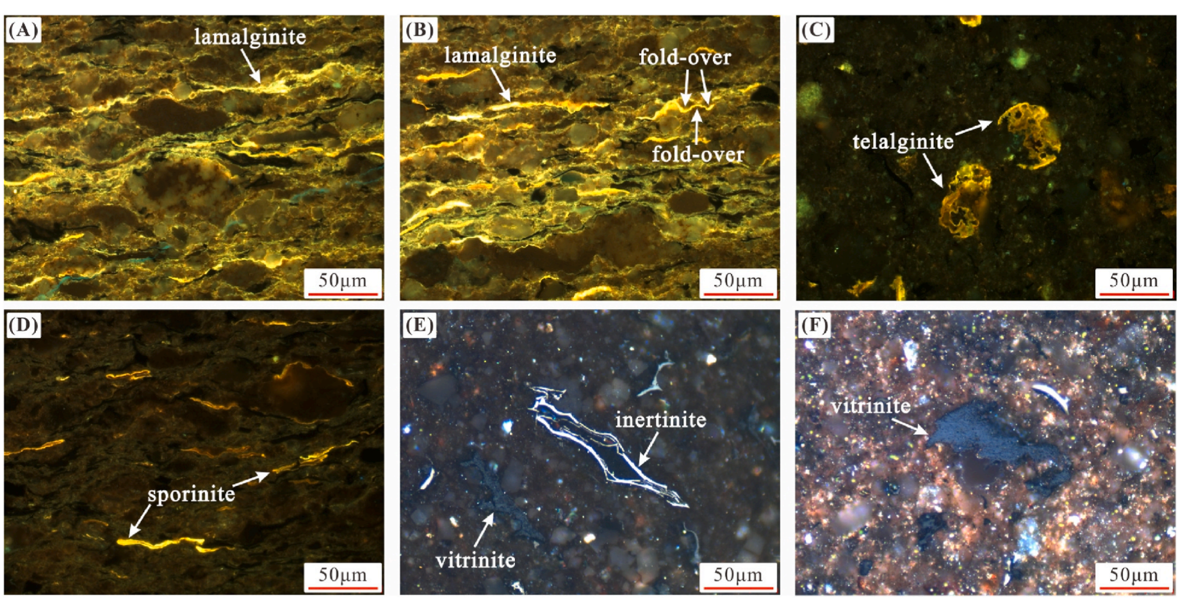


**Fig. 3.** Representative maceral photomicrographs of source rock samples from the $P_2$l. (A) lamalginite, JL-12 under blue light; (B) lamalginite, JL-26 under blue light; (C) telalginite, JL-32 under blue light; (D) sporinite, JL-24 under blue light; (E) inertinite and vitrinite, JL-39 under white light; (F) vitrinite, JL-32 under white light.

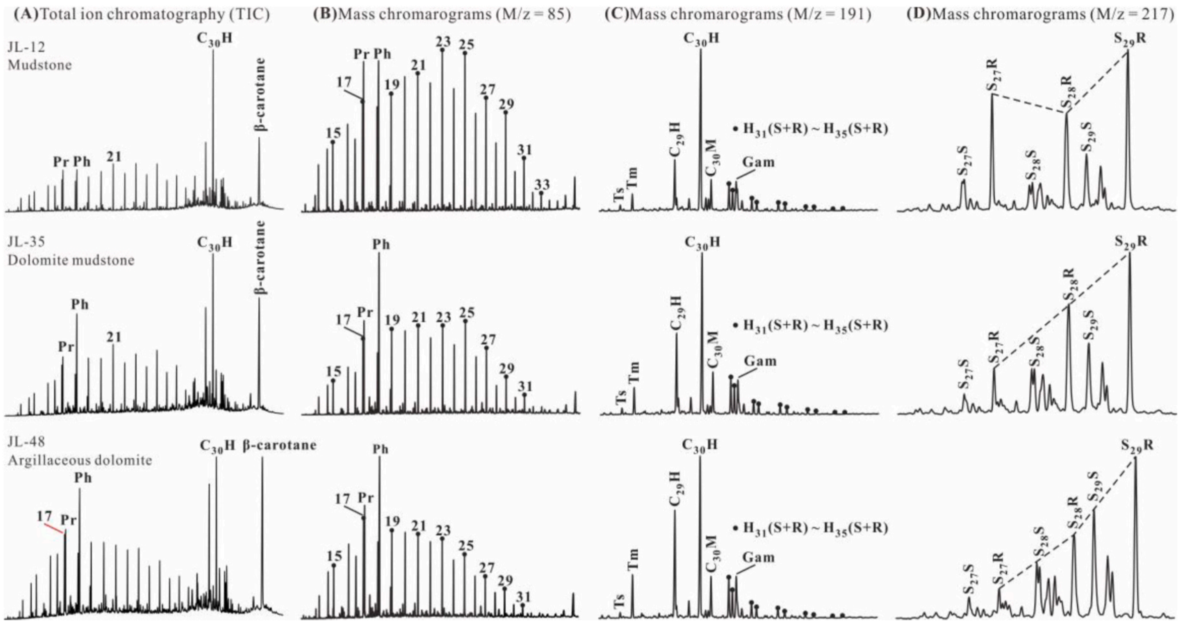

**Fig. 4.** Comparison of saturated hydrocarbon fractions in mudstone, dolomite mudstone and argillaceous dolomite of the $P_2l$. (A) Total ion chromatography (TIC); (B) mass chromatograms (M/z 85); (C) mass chromatograms (M/z 191); (D) mass chromatograms (M/z 217). A key to labelled biomarker in the fragmentgrams is provided in Table 3.

**Table 3**
Abbreviations for labelled biomarker in Fig. 4

| M/z | Abbreviation | Compound |
|---|---|---|
| 85 | 15–33 | $C_{15-33}$ N–alkanes |
| | Pr | Pristane |
| | Ph | Phystane |
| 191 | Ts | 18a(H)–22,29,30–trisnorneohopane |
| | Tm | 17a(H)–22,29,30–trisnorhopane |
| | $C_{29}H$ | 17α(H) 21β(H) $C_{29}$ norhopane |
| | $C_{30}H$ | 17α 21β $C_{30}$ hopane |
| | $C_{30}M$ | 17β 21α $C_{30}$ moretane |
| | Gam | Gammacerane |
| | $H_{31}(S + R)$ | 17α 21β $C_{31}$ hopane (22S) + 17α 21β $C_{31}$ hopane (22R) |
| | $H_{32}(S + R)$ | 17α 21β $C_{32}$ hopane (22S) + 17α 21β $C_{32}$ hopane (22R) |
| | $H_{33}(S + R)$ | 17α 21β $C_{33}$ hopane (22S) + 17α 21β $C_{33}$ hopane (22R) |
| | $H_{34}(S + R)$ | 17α 21β $C_{34}$ hopane (22S) + 17α 21β $C_{34}$ hopane (22R) |
| | $H_{35}(S + R)$ | 17α 21β $C_{35}$ hopane (22S) + 17α 21β $C_{35}$ hopane (22R) |
| 217 | $S_{27}S$–$S_{29}S$ | $C_{27}$–$C_{29}$ ααα 20S sterane |
| | $S_{27}R$–$S_{29}R$ | $C_{27}$–$C_{29}$ ααα 20R sterane |

(Table 4).

#### 4.4.3. Terpanes and their analogues

The hopanes and their analogues in all source rock samples of the $P_2l$ had a similar distribution characteristic. $C_{29}$–$C_{30}$ hopanes and their analogues were dominant compounds, and the relative abundance of homohopanes decrease consistently from $C_{31}$ to $C_{35}$ (Fig. 4C). High abundance of gammacerane was detected in all source rock samples. The gammacerane index, gammacerane/17α21β $C_{30}$ hopane, ranged from 0.06 to 0.36, with an average of 0.23 (Table 4). The mudstone, dolomite mudstone and argillaceous dolomite display significantly different gammacerane index values, with an increasing gammacerane index of 0.06–0.28 (avg. 0.18), 0.18 to 0.31 (avg. 0.25), 0.28 to 0.36 (avg. 0.33) (Fig. 4C and Table 4). 22S/(22S + 22R) $C_{31}$ Hopane ratios, the maturity parameter, is between 0.56 and 0.60 (Table 4), basically reaching the end of isomerization equilibrium.

#### 4.4.4. Steranes and their analogues

The steranes and their analogues were identified in the M/z 217 mass chromatogram. The distribution characteristics of regular steranes in source rocks can indicate the difference in organic matter sources (Bechtel et al., 2012). Previous studies have shown that $C_{27}$ regular steranes are mainly derived from algae and zooplankton (Volkman, 1986). $C_{28}$ regular steranes are mainly derived from plankton containing chlorophyll-c (Volkman, 1986; Grantham and Wakefield, 1988; Zhang et al., 2020), $C_{29}$ regular steranes are mainly derived from higher plants and some brown algae, green algae or cyanobacteria (Huang and Meinschein, 1979). There is an increased relative abundance of $C_{27}$, $C_{28}$ and $C_{29}$ regular steranes in the source rock samples of the $P_2l$ in the Jimsar Sag (Fig. 4D), which is similar to the source rocks of the $P_2l$ in the Santanghu Basin and the Fengcheng Formation in the northwestern margin of the Junggar Basin (Hackley et al., 2016; Gao et al., 2018). There are some differences in the composition characteristics of regular steranes in the $P_2l$ source rocks with different lithologies. The relative abundance of $C_{27}$ regular steranes in mudstone samples varied greatly, ranging from 6.97 to 36.27%, with an average of 17.03%, and the relative abundance of $C_{27}$ regular steranes in some mudstone samples was slightly higher than that of $C_{28}$ regular steranes (Fig. 4D and Table 4). The relative abundance of $C_{27}$ regular steranes in dolomite mudstone (7.94–16.43%, avg. 11.05) and argillaceous dolomite (8.23–11.9%, avg. 9.59%) were relatively low (Fig. 4D and Table 4), indicating that the algae species and their relative composition may be different in the source rocks of different lithologies. The 20S/(20S + 20R) isomerization ratio of $C_{29}$ regular steranes is between 0.27 and 0.54 (avg. 0.42), and the ββ/(ββ+αα) isomerization ratio of the $C_{29}$ regular steranes is between 0.21 and 0.40 (avg. 0.30) (Table 4), which is consistent with the thermal evolution indicated by $T_{max}$ and *Ro*.

### 4.5. Elemental geochemistry

The analysis results of major and trace elements of various rocks in the $P_2l$ in the study area are shown in Table 5. All samples are mainly composed of $SiO_2$, $Al_2O_3$, CaO and MgO (57.53%, 11.90%, 9.20% and 6.55%). There are obvious differences in the composition of major elements between the source rocks with different lithologies. The mudstone, dolomitic mudstone and argillaceous dolomite are enriched in MgO to varying degrees, which are 1.20%–7.12% (avg. 3.19%), 4.74% to 10.10% (avg. 7.54%), 11.48% to 14.29% (avg. 12.41%). In addition, the CaO content in mudstone, dolomitic mudstone and

**Table 4**
Saturate biomarker ratios of the samples from the Lucaogou Formation, Jimsar Sag.

| Sample | Lithology | 1 | 2 | 3 | 4 | 5 | 6 | 7 | 8 | 9 | 10 | 11 | 12 | 13 |
|---|---|---|---|---|---|---|---|---|---|---|---|---|---|---|
| JL-3 | A | 1.15 | 0.72 | 1.02 | 0.88 | 1.10 | 0.39 | 0.21 | 0.58 | 15.85 | 41.55 | 42.59 | 0.50 | 0.40 |
| JL-4 | A | 1.18 | 0.75 | 1.06 | 0.86 | 1.16 | 0.38 | 0.18 | 0.59 | 14.24 | 39.58 | 46.17 | 0.47 | 0.38 |
| JL-6 | A | 1.18 | 0.72 | 0.98 | 0.78 | 1.18 | 0.34 | 0.20 | 0.59 | 16.02 | 37.28 | 46.71 | 0.46 | 0.36 |
| JL-8 | A | 1.28 | 1.27 | 0.78 | 0.65 | 1.28 | 0.29 | 0.16 | 0.58 | 16.84 | 37.30 | 45.87 | 0.45 | 0.33 |
| JL-9 | A | 1.31 | 1.37 | 1.68 | 2.64 | 0.90 | 0.66 | 0.27 | 0.59 | 6.97 | 41.90 | 51.13 | 0.48 | 0.37 |
| JL-10 | A | 1.28 | 1.06 | 1.71 | 2.30 | 0.87 | 0.52 | 0.25 | 0.59 | 9.68 | 44.40 | 45.91 | 0.54 | 0.40 |
| JL-12 | A | 1.63 | 1.12 | 2.58 | 2.49 | 1.19 | 0.59 | 0.11 | 0.56 | 26.04 | 31.80 | 42.16 | 0.27 | 0.22 |
| JL-15 | A | 1.32 | 0.69 | 1.13 | 0.66 | 1.06 | 0.22 | 0.16 | 0.60 | 13.60 | 28.81 | 57.59 | 0.34 | 0.24 |
| JL-17 | A | 1.85 | 1.33 | 2.10 | 1.98 | 0.93 | 0.20 | 0.14 | 0.57 | 19.88 | 35.96 | 44.16 | 0.27 | 0.22 |
| JL-18 | A | 1.40 | 0.96 | 1.43 | 0.93 | 1.34 | 0.68 | 0.12 | 0.60 | 24.64 | 29.42 | 45.94 | 0.37 | 0.25 |
| JL-19 | A | 1.43 | 1.12 | 2.42 | 2.04 | 1.21 | 0.15 | 0.06 | 0.59 | 36.27 | 26.92 | 36.81 | 0.47 | 0.31 |
| JL-22 | A | 1.38 | 1.00 | 1.98 | 3.10 | 0.83 | 1.07 | 0.22 | 0.58 | 11.47 | 39.27 | 49.27 | 0.46 | 0.28 |
| JL-23 | A | 1.35 | 1.10 | 2.34 | 3.36 | 0.92 | 1.78 | 0.28 | 0.58 | 9.89 | 37.68 | 52.43 | 0.47 | 0.31 |
| JL-25 | B | 1.19 | 0.89 | 1.50 | 1.73 | 0.96 | 0.53 | 0.26 | 0.58 | 9.40 | 43.82 | 46.78 | 0.52 | 0.40 |
| JL-26 | B | 1.52 | 1.47 | 1.39 | 1.99 | 1.05 | 0.63 | 0.28 | 0.58 | 8.95 | 42.60 | 48.45 | 0.49 | 0.35 |
| JL-28 | B | 1.30 | 1.49 | 1.08 | 1.49 | 1.07 | 0.79 | 0.23 | 0.58 | 7.94 | 40.50 | 51.56 | 0.45 | 0.37 |
| JL-33 | B | 1.43 | 1.69 | 1.05 | 1.55 | 1.14 | 0.72 | 0.28 | 0.57 | 11.27 | 41.63 | 47.10 | 0.35 | 0.21 |
| JL-34 | B | 1.66 | 1.85 | 2.38 | 4.94 | 0.93 | 1.30 | 0.31 | 0.56 | 12.53 | 38.25 | 49.23 | 0.34 | 0.22 |
| JL-35 | B | 1.63 | 0.80 | 2.42 | 4.21 | 0.75 | 1.32 | 0.20 | 0.56 | 10.84 | 41.80 | 47.36 | 0.34 | 0.23 |
| JL-37 | B | 1.43 | 0.78 | 1.84 | 1.58 | 1.09 | 0.51 | 0.18 | 0.58 | 16.43 | 43.21 | 40.36 | 0.41 | 0.25 |
| JL-42 | C | 1.65 | 1.08 | 2.34 | 6.39 | 0.77 | 1.38 | 0.35 | 0.58 | 9.78 | 39.10 | 51.12 | 0.39 | 0.23 |
| JL-43 | C | 1.44 | 0.81 | 1.30 | 1.45 | 1.10 | 0.88 | 0.28 | 0.56 | 11.39 | 39.75 | 48.87 | 0.34 | 0.23 |
| JL-44 | C | 1.38 | 1.31 | 0.86 | 0.58 | 1.36 | 0.69 | 0.36 | 0.58 | 8.23 | 34.73 | 57.04 | 0.37 | 0.26 |
| JL-48 | C | 1.44 | 1.27 | 2.40 | 4.02 | 0.86 | 1.91 | 0.33 | 0.58 | 8.96 | 38.35 | 52.69 | 0.46 | 0.28 |

Note: A. Mudstone; B. Dolomitic mudstone; C. Argillaceous dolomite; 1. CPI (Scalan and Smith, 1970); 2. $\Sigma NC_{21}^{-}/\Sigma NC_{22}^{+}$; 3. $Pr/NC_{17}$; 4. $Ph/NC_{18}$; 5. Pr/Ph; 6. β–carotene index = 100 × (β–carotane/17α 21β $C_{30}$ hopane) (Martins et al., 2020); 7. GI: gammacerane index = gammacerane/17α 21β $C_{30}$ hopane (Moldowan et al., 1985; Sinninghe Damsté et al., 1995); 8. 22S/(22S + 22R) $C_{31}$ Hopanes; 9. $C_{27}/(C_{27} + C_{28} + C_{29})$ regular steranes (%); 10. $C_{28}/(C_{27} + C_{28} + C_{29})$ regular steranes (%); 11. $C_{29}/(C_{27} + C_{28} + C_{29})$ regular steranes (%); 12. 20S/(20S + 20R) $C_{29}$ Steranes; 13. ββ/(αα + ββ) $C_{29}$ Steranes.

argillaceous dolomite increases successively, with the contents ranging from 0.67% to 11.09% (avg. 3.70%), 7.01% to 15.95% (avg. 11.41%), and 16.23% to 21.30% (avg. 17.54%), respectively (Table 5).

There are obvious differences in trace elements among the source rocks with different lithologies. Compared with mudstone (Sr: 95–623 ppm,avg. 267 ppm; Ba: 153–511 ppm, 377 ppm), dolomite mudstone and argillaceous dolomite have higher Sr content (358–878 ppm, avg. 616 ppm; 528–1425 ppm, avg. 924 ppm) and lower Ba content (284–438 ppm, avg. 350 ppm; 188–412 ppm, avg. 296 ppm). The Sr/Ba ratios of dolomite mudstones (0.82–2.50, avg. 1.80) and argillaceous dolomite (2.37–3.64, avg. 3.06) are also higher than those of mudstones (0.21–1.41, avg. 0.74). In addition, compared with mudstones, the Sr/Cu ratios of dolomite mudstones and argillaceous dolomite are relatively higher, while the C values and Rb/Sr ratios reflecting paleoclimate are lower (Table 5). C-value = Σ(Fe + Mn + Cr + Ni + V + Co)/Σ(Ca + Mg + Sr + Ba + K + Na) (Turgeon and Brumsack, 2006; Algeo and Tribovillard, 2009).

## 5. Discussion

### 5.1. Sediment provenances

The elemental and mineral composition of clastic rocks is controlled by their provenance, which may be composed of igneous, sedimentary, and metamorphic rocks, or a mixture of different proportions of these rocks, consequently, it is important to trace the provenance of clastic rocks (Condie et al., 2001). At present, geochemical parameters of elements are widely used to determine the sedimentary provenance of fine-grained sediments (Cullers, 1995; Moradi et al., 2016). Compared with acid rocks, basic rocks are generally enriched in Sc and depleted in Th. In addition, Zr is enriched in heavy mineral zircons, while Sc remains unchanged during recycling. Therefore, the crossplot of Th/Sc–Zr/Sc can be used to determine the provenances and recycling conditions of sediments (McLennan et al., 1993). The ratios of Th/Sc in mudstone, dolomite mudstone and argillaceous dolomite in the $P_2l$ are 0.33–0.64 (avg. 0.46), 0.43–1.40 (avg. 0.81) and 0.63–1.53 (avg. 0.87), and the Zr/Sc values are 6.19–15.61 (avg. 11.31), 6.34–12.92 (avg. 9.83) and 6.22–13.93 (avg. 11.14), respectively (Table 5), indicating more felsic sources and no recycling (Fig. 5A).

The oxides and hydroxides of Al- and Ti- have a low-solubility in low-temperature aqueous solutions, which retain the characteristics of parent rock after geological alternation. Therefore, The ratio of $Al_2O_3/TiO_2$ is an effective parameter to indicate sediment provenance (Stumm and Morgan, 1981; Hayashi et al., 1997; Moradi et al., 2016). The $Al_2O_3/TiO_2$ ratios (<8, 8–21, and >21) correspond to mafic, intermediate and felsic igneous rocks (Hayashi et al., 1997). The $Al_2O_3/TiO_2$ ratios of mudstone, dolomitic mudstone and argillaceous dolomite of $P_2l$ in the study area are 17.79–53.61 (avg. 27.20), 15.62–34.39 (avg. 24.12) and 18.89–38.29 (avg. 26.45), respectively (Table 5), indicating that the sediment provenances of these rocks are felsic igneous rocks (Fig. 5B). Previous studies have shown that the sediment provenances of the $P_2l$ source rocks in Jimsar Sag was mainly from two provenance regions of the Shaqi and Santai uplifts (Tao et al., 2016), which are located in the north and south of the sag, respectively (Fig. 1C). During the sedimentary period of the $P_2l$, the basin was mainly a saline lacustrine environment. Carbonate were derived from the chemical deposits in the basin, and volcanic debris particles were derived from the volcanic materials that were transported into the lake by wind or water during volcanic activity. The eventful volcanic activity provided special sediment provenances, which increased the complexity of mixed sediments in the study area (Zhang et al., 2019a; Wu et al., 2022).

### 5.2. Palaeoenvironment and its impact on organic enrichment

#### 5.2.1. Paleoclimate

Paleoclimate can influence the depositional process and organic matter enrichment by controlling the physical and chemical properties of lacustrine basins (Tanaka et al., 2007; Bai et al., 2015; Hakimi et al., 2016). Sr/Cu and Rb/Sr ratios are effective paleoclimatic indicators, which are commonly used for paleoclimate reconstruction during the deposition of fine-grained sediments (Lerman, 1978; Sawyer, 1986; Zhao et al., 2007; Moradi et al., 2016). Sr is preferentially enriched under arid conditions, while Cu is enriched under humid conditions (Lerman, 1978; Cao et al., 2015). Sr/Cu ratios of 1.0–5.0, 5.0–10.0 and

**Table 5**
Element ratios of the samples from the Lucaogou Formation, Jimsar Sag.

| Sample | Lithology | 1 | 2 | 3 | 4 | 5 | 6 | 7 | 8 | 9 | 10 | 11 | 12 | 13 | 14 | 15 | 16 | 17 | 18 | 19 | 20 | 21 | 22 | 23 | 24 |
|---|---|---|---|---|---|---|---|---|---|---|---|---|---|---|---|---|---|---|---|---|---|---|---|---|---|
| JL-1 | A | 57.79 | 15.62 | 4.43 | 3.43 | 0.88 | 17.79 | 214 | 426 | 8.18 | 0.45 | 0.42 | 1.80 | 0.54 | 0.50 | 3.07 | 2.66 | 1.69 | 0.69 | 14.39 | 6.17 | 27.46 | 20.75 | 11.20 | 0.23 |
| JL-2 | A | 67.11 | 15.19 | 0.67 | 1.26 | 0.61 | 24.75 | 95 | 462 | 12.37 | 0.64 | 0.28 | 3.46 | 0.45 | 0.21 | 1.28 | 1.00 | 1.58 | 0.73 | 3.43 | 3.42 | 8.62 | 11.25 | 7.63 | 0.25 |
| JL-5 | A | 63.53 | 14.38 | 0.72 | 1.89 | 0.39 | 37.08 | 108 | 311 | 10.55 | 0.33 | 0.37 | 4.52 | 0.34 | 0.35 | 0.81 | 1.11 | 1.62 | 0.70 | 3.14 | 3.79 | 9.64 | 17.74 | 16.77 | 0.19 |
| JL-7 | A | 61.96 | 15.36 | 0.86 | 2.40 | 0.53 | 29.10 | 231 | 428 | 6.19 | 0.47 | 0.34 | 2.92 | 0.60 | 0.54 | 1.28 | 2.44 | 1.63 | 0.72 | 9.71 | 5.46 | 16.35 | 16.08 | 5.68 | 0.15 |
| JL-8 | A | 68.67 | 16.35 | 0.80 | 1.20 | 0.66 | 24.68 | 101 | 305 | 11.87 | 0.40 | 0.46 | 1.79 | 0.73 | 0.33 | 1.01 | 1.47 | 1.67 | 0.70 | 6.50 | 4.45 | 21.25 | 19.23 | 11.25 | 0.15 |
| JL-9 | A | 80.82 | 6.55 | 3.09 | 2.62 | 0.22 | 29.27 | 207 | 153 | 7.61 | 0.53 | 0.30 | 5.39 | 0.14 | 1.35 | 1.53 | 1.26 | 1.39 | 0.73 | 11.08 | 5.91 | 21.93 | 19.22 | 19.85 | 0.24 |
| JL-11 | A | 56.77 | 10.18 | 11.09 | 7.12 | 0.55 | 18.50 | 388 | 449 | 14.99 | 0.37 | 0.33 | 3.96 | 0.17 | 0.86 | 4.32 | 1.86 | 1.73 | 0.73 | 18.19 | 9.65 | 38.05 | 32.23 | 15.65 | 0.29 |
| JL-13 | A | 64.57 | 13.71 | 5.27 | 2.49 | 0.53 | 25.79 | 313 | 358 | 11.50 | 0.39 | 0.31 | 5.07 | 0.14 | 0.87 | 1.52 | 0.94 | 1.48 | 0.69 | 8.50 | 5.69 | 20.25 | 22.94 | 13.57 | 0.22 |
| JL-14 | A | 59.39 | 15.06 | 3.40 | 3.35 | 0.28 | 53.61 | 527 | 374 | 15.61 | 0.35 | 0.25 | 6.66 | 0.09 | 1.41 | 2.03 | 1.77 | 1.83 | 0.65 | 9.92 | 6.53 | 24.58 | 18.73 | 7.08 | 0.27 |
| JL-16 | A | 58.11 | 12.10 | 5.12 | 4.26 | 0.67 | 18.05 | 623 | 446 | 12.10 | 0.63 | 0.22 | 7.90 | 0.08 | 1.40 | 2.71 | 1.17 | 1.42 | 0.76 | 12.32 | 5.98 | 20.14 | 22.54 | 21.23 | 0.24 |
| JL-20 | A | 67.22 | 14.56 | 2.30 | 3.68 | 0.69 | 21.14 | 183 | 299 | 12.35 | 0.36 | 0.38 | 2.58 | 0.31 | 0.61 | 2.57 | 1.48 | 1.78 | 0.65 | 9.21 | 6.24 | 19.72 | 13.76 | 5.62 | 0.17 |
| JL-21 | A | 59.62 | 14.81 | 6.68 | 4.63 | 0.56 | 26.65 | 216 | 511 | 12.38 | 0.54 | 0.36 | 2.12 | 0.38 | 0.42 | 4.25 | 2.35 | 1.69 | 0.68 | 13.01 | 7.44 | 30.49 | 25.12 | 17.73 | 0.21 |
| JL-24 | B | 59.74 | 11.55 | 9.27 | 6.87 | 0.34 | 34.39 | 362 | 394 | 9.43 | 0.65 | 0.30 | 7.97 | 0.14 | 0.92 | 2.68 | 2.21 | 1.76 | 0.74 | 7.43 | 6.12 | 12.74 | 11.27 | 24.70 | 0.24 |
| JL-26 | B | 52.59 | 8.87 | 13.85 | 8.13 | 0.30 | 29.75 | 702 | 334 | 8.83 | 0.74 | 0.20 | 10.29 | 0.12 | 2.10 | 1.49 | 1.54 | 1.36 | 0.78 | 14.52 | 7.39 | 31.30 | 22.78 | 30.88 | 0.26 |
| JL-27 | B | 52.81 | 11.33 | 10.67 | 8.42 | 0.48 | 23.66 | 465 | 284 | 10.33 | 1.40 | 0.24 | 12.60 | 0.17 | 1.64 | 1.77 | 2.92 | 1.61 | 0.81 | 6.15 | 4.07 | 7.25 | 12.90 | 16.67 | 0.33 |
| JL-28 | B | 52.83 | 10.74 | 11.62 | 9.54 | 0.41 | 26.46 | 878 | 376 | 9.50 | 0.49 | 0.16 | 12.25 | 0.06 | 2.34 | 1.18 | 0.83 | 1.33 | 0.74 | 12.61 | 5.95 | 22.69 | 24.55 | 29.20 | 0.28 |
| JL-29 | B | 55.61 | 9.86 | 8.73 | 7.18 | 0.61 | 16.07 | 713 | 285 | 6.34 | 0.97 | 0.18 | 13.61 | 0.07 | 2.50 | 4.19 | 3.43 | 1.59 | 0.80 | 10.04 | 4.86 | 17.73 | 16.37 | 18.04 | 0.27 |
| JL-30 | B | 60.83 | 10.88 | 7.25 | 5.80 | 0.53 | 20.44 | 785 | 343 | 10.24 | 0.65 | 0.18 | 16.29 | 0.10 | 2.29 | 2.33 | 1.20 | 1.62 | 0.78 | 8.37 | 5.75 | 11.98 | 11.55 | 26.39 | 0.32 |
| JL-31 | B | 60.55 | 12.23 | 7.01 | 4.74 | 0.46 | 26.62 | 358 | 438 | 12.92 | 1.06 | 0.31 | 10.07 | 0.15 | 0.82 | 2.13 | 2.32 | 1.61 | 0.75 | 5.49 | 4.96 | 8.62 | 15.83 | 11.74 | 0.29 |
| JL-32 | B | 51.41 | 10.32 | 15.95 | 10.10 | 0.41 | 24.97 | 520 | 357 | 8.14 | 0.75 | 0.24 | 10.92 | 0.13 | 1.46 | 4.18 | 4.16 | 1.77 | 0.79 | 8.72 | 5.71 | 19.59 | 15.89 | 34.42 | 0.36 |
| JL-36 | B | 57.39 | 10.21 | 13.44 | 6.35 | 0.40 | 25.62 | 588 | 323 | 7.77 | 0.86 | 0.17 | 12.21 | 0.04 | 1.82 | 3.85 | 1.73 | 1.49 | 0.71 | 8.91 | 6.54 | 31.26 | 15.48 | 10.84 | 0.24 |
| JL-38 | B | 56.91 | 12.63 | 13.06 | 9.14 | 0.81 | 15.62 | 738 | 376 | 12.36 | 0.43 | 0.20 | 10.37 | 0.07 | 1.96 | 2.81 | 1.68 | 1.75 | 0.76 | 10.65 | 5.74 | 21.08 | 18.70 | 20.33 | 0.25 |
| JL-39 | B | 53.52 | 9.86 | 14.64 | 6.69 | 0.45 | 21.77 | 671 | 336 | 12.29 | 0.86 | 0.15 | 11.63 | 0.09 | 2.00 | 6.35 | 2.68 | 1.77 | 0.72 | 11.06 | 6.63 | 28.37 | 13.52 | 36.80 | 0.21 |
| JL-40 | C | 50.29 | 9.07 | 16.23 | 11.49 | 0.39 | 22.97 | 1157 | 380 | 11.90 | 0.77 | 0.14 | 18.51 | 0.03 | 3.04 | 3.76 | 2.30 | 1.64 | 0.77 | 13.02 | 7.02 | 24.45 | 21.07 | 31.24 | 0.34 |
| JL-41 | C | 43.78 | 8.26 | 21.30 | 14.29 | 0.44 | 18.89 | 949 | 261 | 6.22 | 0.63 | 0.11 | 22.60 | 0.03 | 3.64 | 0.91 | 0.96 | 1.37 | 0.72 | 9.61 | 5.88 | 14.87 | 12.46 | 53.08 | 0.42 |
| JL-45 | C | 49.09 | 12.26 | 14.03 | 11.48 | 0.51 | 23.81 | 562 | 237 | 13.93 | 1.53 | 0.18 | 17.38 | 0.05 | 2.37 | 2.59 | 1.44 | 1.49 | 0.65 | 4.98 | 5.48 | 13.14 | 13.28 | 42.36 | 0.29 |
| JL-46 | C | 41.76 | 13.45 | 18.01 | 12.90 | 0.35 | 38.29 | 1425 | 412 | 12.97 | 0.65 | 0.14 | 18.61 | 0.02 | 3.46 | 3.92 | 2.49 | 1.71 | 0.68 | 10.75 | 7.20 | 30.33 | 22.07 | 42.55 | 0.35 |
| JL-47 | C | 46.28 | 7.78 | 18.14 | 11.88 | 0.27 | 28.30 | 528 | 188 | 10.70 | 0.79 | 0.19 | 19.79 | 0.06 | 2.81 | 3.07 | 4.00 | 1.80 | 0.73 | 6.48 | 6.12 | 19.90 | 15.58 | 35.20 | 0.31 |

Note: A. Mudstone; B. Dolomitic mudstone; C. Argillaceous dolomite; 1. $SiO_2$ (%); 2. $Al_2O_3$ (%); 3. CaO (%); 4. MgO (%); 5. $TiO_2$ (%); 6. $Al_2O_3/TiO_2$; 7. Sr (ppm); 8. Ba (ppm); 9. Zr/Sc; 10. Th/Sc; 11. C-value; 12. Sr/Cu; 13. Rb/Sr; 14. Sr/Ba; 15. $Mo_{EF}$; 16. $U_{EF}$; 17. δU; 18. V/(V + Ni); 19. Cu/Al; 20. Ni/Al; 21. Zn/Al; 22. $Zr/Al_2O_3$; 23. Li/Al; 24. Cr/Zr.

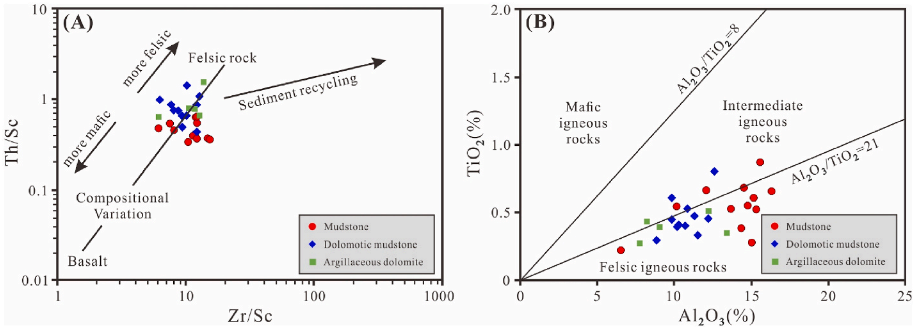


**Fig. 5.** Crossplots of sedimentary provenances of source rock samples from the $P_2l$ in Jimsar Sag. (A) Th/Sc versus Zr/Sc (according to McLennan et al., 1993); (B) $TiO_2$ versus $Al_2O_3$ (according to Hayashi et al., 1997).

> 10.0 correspond to warm–humid conditions, semi-arid–humid conditions and arid–hot conditions, respectively (Lerman, 1978; Liu and Zhou, 2007). The Sr/Cu ratios of the $P_2l$ mudstone, dolomitic mudstone and argillaceous dolomite are 1.79–7.90 (avg. 4.01), 7.97–16.29 (avg. 11.66) and 17.38–22.60 (avg. 19.38) respectively (Table 5), indicating that mudstone was formed under warm-humid and semi-arid-humid conditions, dolomitic mudstone was formed under semi-arid-humid and arid-hot conditions, and argillaceous dolomite was formed under arid-hot conditions. The ratios of Rb/Sr increase as the climate becomes more humid (Jin and Zhang, 2002; Bai et al., 2015; Wu et al., 2021). The Rb/Sr ratios of the $P_2l$ mudstone are significantly different from those of the other two types of source rocks in the study area. Compared with mudstone (0.08–0.73, avg. 0.33), the lower Rb/Sr ratios of dolomite mudstone (0.04–0.17, avg. 0.10) and argillaceous dolomite (0.02–0.06, avg. 0.04) also suggest relatively arid paleoclimate (Table 5).

The C value is used to evaluate paleoclimatic changes (Zhao et al., 2007; Moradi et al., 2016; Tao et al., 2017). C-value = Σ(Fe + Mn + Cr + Ni + V + Co)/Σ(Ca + Mg + Sr + Ba + K + Na) (Turgeon and Brumsack, 2006; Algeo and Tribovillard, 2009). High C values (C-value >0.8) reflect humid paleoclimate, low C values (C-value <0.2) reflect arid paleoclimate, and those range from 0.2 to 0.4, 0.4 to 0.6 and 0.6 to 0.8 reflect semiarid, semiarid to semihumid, and semihumid paleoclimate, respectively (Qiu et al., 2015; Moradi et al., 2016; Y. Zhang et al., 2020). The C values of the source rock with different lithologies in the $P_2l$ are different (Fig. 6A). Compared with dolomitic mudstone and argillaceous dolomite, mudstone has higher C-values, ranging from 0.17 to 0.53 (avg. 0.33), indicating that most mudstones were deposited in semiarid and semiarid to semihumid paleoclimate; The C-values of dolomitic mudstones ranging from 0.13 to 0.31 (avg. 0.20), indicating an arid and semiarid paleoclimate; Argillaceous dolomite, with low C-values ranging from 0.09 to 0.19 (avg. 0.14), were formed under arid paleoclimate (Table 5).

The above analysis shows that the $P_2l$ source rocks in the Jimsar Sag were formed in an arid and hot paleoclimatic condition, which were similar to the $P_2l$ in the Santanghu Basin deposited at the same time (Qi et al., 2013; Zhang et al., 2018b; Pan et al., 2020), and is consistent with previous studies (Qu et al., 2019; Liu et al., 2019). This study further confirmed that mudstone, dolomitic mudstone and argillaceous dolomite were formed in different paleoclimatic conditions. Based on C-values, Sr/Cu and Rb/Sr ratios, it is clear that mudstone is mainly formed under warm-humid and semi-arid-humid conditions, dolomitic mudstone is mainly formed under semi-arid-humid and arid-hot conditions, and argillaceous dolomite is mainly formed under arid-hot conditions. Further analysis (Fig. 7A–C) shows that there is no significant

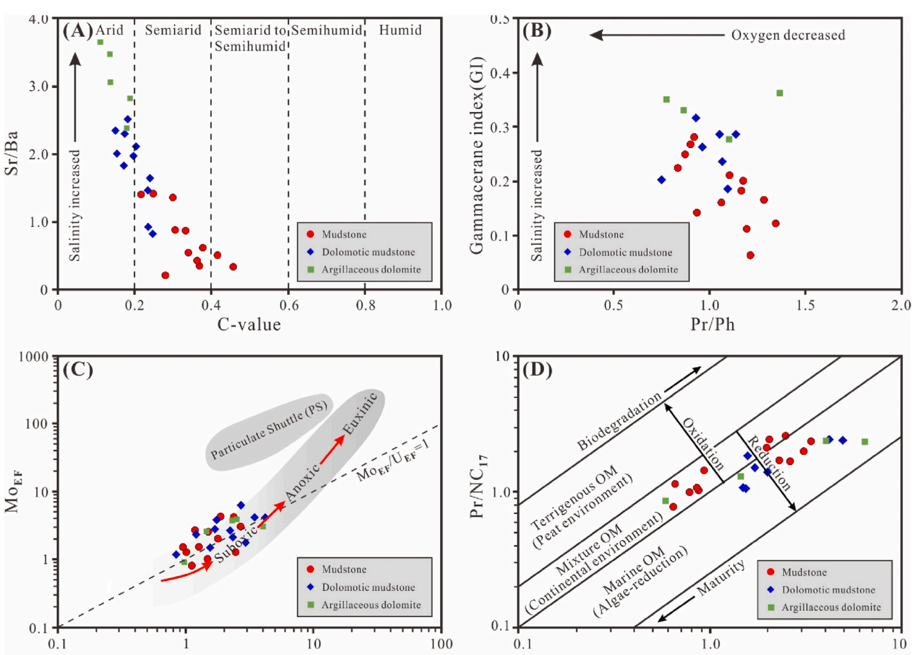


**Fig. 6.** Crossplots of paleo-environmental parameters of source rock samples from the $P_2l$ in Jimsar Sag. (A) Sr/Ba versus C-value; (B) Gammacerane index (GI) versus Pr/Ph; (C) $Mo_{EF}$ versus $U_{EF}$ (modified from Algeo and Tribovillard, 2009); (D) $Pr/NC_{17}$ versus $Ph/NC_{18}$ (according to Connan and Cassou, 1980).

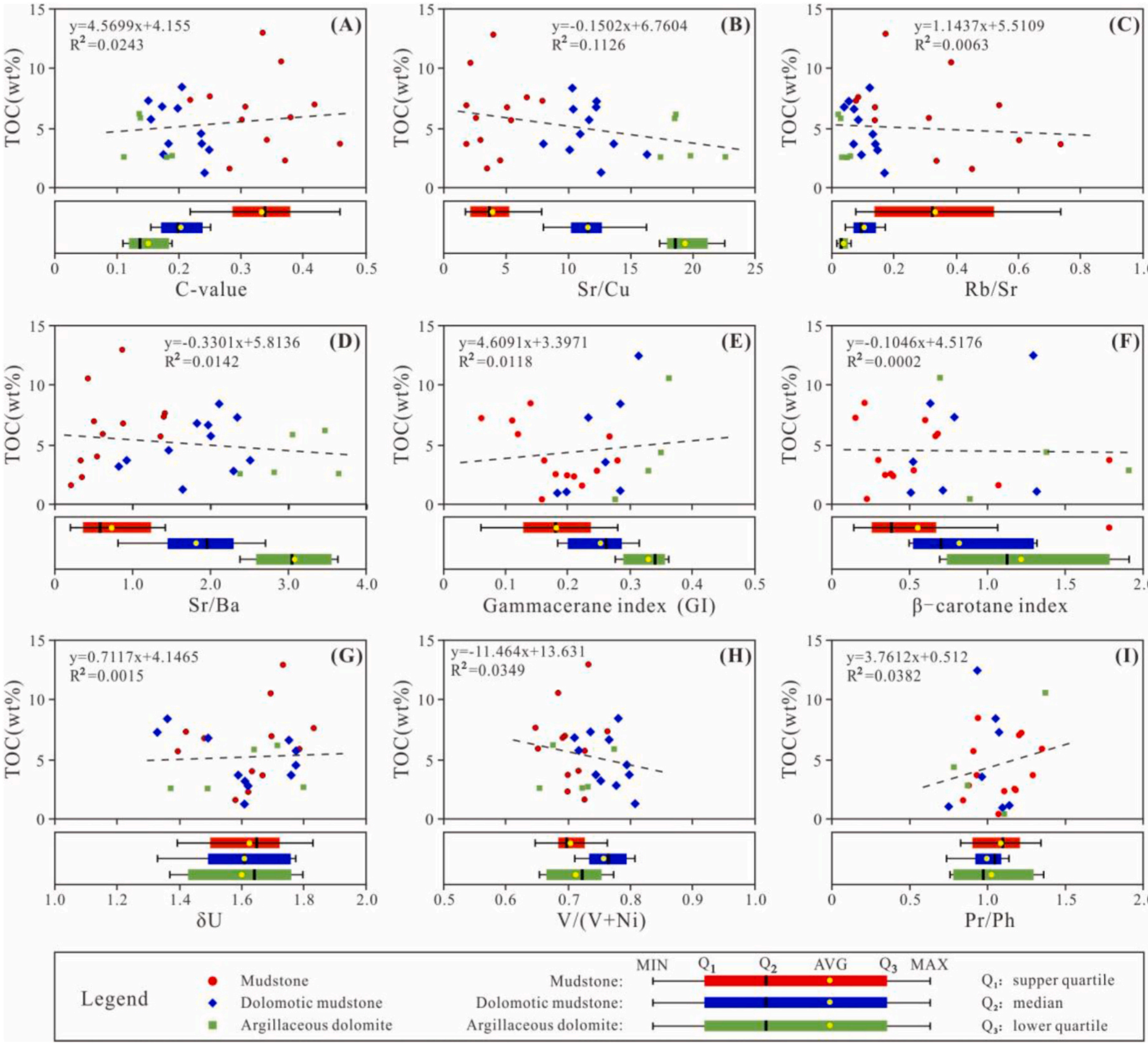


**Fig. 7.** The correlation between TOC and paleoclimate parameter (A–C: C-value, Sr/Cu, Rb/Sr), paleosalinity parameter (D–F: Sr/Ba, Gammacerane index, β-carotane index), and redox indicators (G–I: δU, V/(V + Ni), Pr/Ph) of source rock samples from the $P_2l$ in Jimsar Sag.

correlation between TOC and paleoclimate parameters in $P_2l$ source rocks, suggesting that paleoclimate changes did not cause significant changes in the organic matter enrichment degree of the $P_2l$ source rocks in the study area.

Although the paleoclimate has no direct influence on the organic matter enrichment of source rocks in the $P_2l$, it plays a crucial role in the formation of dolomite. As shown in Fig. 8A and B, a decrease in C values and an increase in Sr/Cu ratios correspond to an increase in the content of dolomite within source rocks, indicating that the arid paleoclimate is conducive to the development of dolomite. These trends suggest that paleoclimate controlled the formation of dolomite. In addition, the formation of dolomite requires harsh physical and chemical conditions (Lippmann, 1973; Brauchli et al., 2015), the first condition is a high Mg/Ca ratio of the water column, and the second is to break the rigid hydration shell around $Mg^{2+}$ under microbial activity or high temperature conditions (Lippmann, 1973; Petrash et al., 2017; Cheng et al., 2021). During the deposition period of the $P_2l$, frequent hydrothermal activity in the study area could provide a large amount of $Mg^{2+}$ (Nishiyama et al., 2001; Kenward et al., 2009; Zhang et al., 2015; Rakocinski et al., 2018; Meng et al., 2022). Under the arid-hot paleoclimate condition, the evaporation of lake water leads to the increase of the $Mg^{2+}$ concentration of water and Mg/Ca ratio, which was conducive to the precipitation of dolomite (Sadooni et al., 2010; Dunham et al., 2020; Wu et al., 2022). In addition, recent studies have shown that frequent hydrothermal and microbial activity during the sedimentary period of the $P_2l$ also play an important role in the formation of dolomite (Zhang et al., 2018a; Sun et al., 2021, 2022; Wu et al., 2022). The hydrothermal activity raised the heat flow background value of the lake basin, and high temperature hydrothermal condition breaks the dynamic barrier of dolomite formation (Zhang et al., 2018a; Wu et al., 2022). The metabolic activity of microorganisms can increase the pH value of fluid, $CO_3^{2-}$ concentration and decrease $SO_4^{2-}$ concentration, which is beneficial to the precipitation of dolomite at a normal temperature (Slaughter and Hill, 1991; Wright, 1997; Warthmann et al., 2000; Kenward et al., 2009; Sun et al., 2021, 2022). In conclusion, hydrothermal fluids and microbial activity may have provided suitable thermodynamic and dynamic conditions for the formation of dolomite, and the periodic change of paleoclimate is the main factor that causes the frequent interbedding distribution of fine grained rocks (mudstone, dolomitic mudstone and argillaceous dolomite) with different dolomite content in the $P_2l$.

### 5.2.2. *Paleosalinity*

Salinity has a significant influence on the paleoenvironment and organic matter accumulation of lacustrine systems (Ma et al., 2016; Pan et al., 2020; Wu et al., 2021). Salinity can exert a crucial control on the water column stratification of lacustrine systems, thereby influencing the redox environment at the bottom of the lake (Eugster and Hardie, 1978; Wei et al., 2018). Generally, the bottom of the saline lake basin

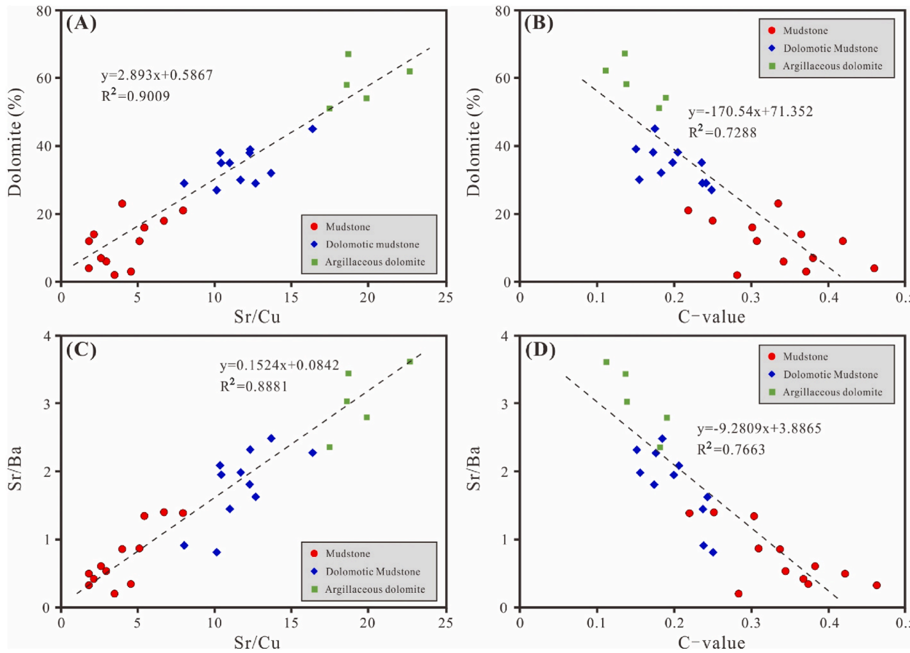


**Fig. 8.** The correlation of paleoclimate parameter (Sr/Cu; C-value) versus dolomite content and Sr/Ba of source rock samples from the $P_2l$ in Jimsar Sag.

forms a reducing environment with good preservation conditions, which is conducive to the deposition of organic-rich source rocks (Ma et al., 2016; Pan et al., 2020). In this study, Sr/Ba ratio and gammacerane index are used to evaluate paleosalinity.

Most studies have demonstrated that the Sr/Ba is widely used to evaluate the salinity of water bodies, the ratios of >1.0, 1.0–0.6, and <0.6 were indicative of salt water, brackish water, and freshwater (Rohling, 2000; Custodio, 2002; Zhang et al., 2018b). The Sr/Ba ratios in mudstone, dolomitic mudstone and argillaceous dolomite of the $P_2l$ are 0.21–1.41 (avg. 0.74), 0.82–2.50 (avg. 1.80) and 2.37–3.64 (avg. 3.06), respectively (Table 5), indicating that the salinity of water column increased gradually during the sedimentary period from mudstone, dolomitic mudstone to argillaceous dolomite. Mudstone was deposited in freshwater to saline water environments, dolomitic mudstone was deposited in brackish to saline water environments, and argillaceous dolomite was deposited in saline water environments. Although the gammacerane index and β-carotane index cannot be used directly to indicate the salinity of the water column, a high abundance of gammacerane tends to indicate saline and stratified water columns (Sinninghe Damsté et al., 1995; Liu et al., 2017; Martins et al., 2020; Xia et al., 2021), and a high abundance of β-carotane is often associated with evaporation, high salinity, and anoxic environments (Murphy et al., 1967; Hopmans et al., 2005; Ding et al., 2020; Peters et al., 2005; Xia et al., 2021). As shown in Figs. 6B and 7E and F, the gammacerane index and β-carotane index of mudstone, dolomitic mudstone and argillaceous dolomite indicate that they were deposited in a saline and stratified water column. In addition, the salinity of the water column increases successively during the sedimentary period from mudstone, dolomitic mudstone to argillaceous dolomite.

In conclusion, source rocks of the $P_2l$ in the Jimsar Sag were deposited under a saline and stratified water column, which is consistent with previous studies (Su et al., 2019b; Zhang et al., 2019a; Ding et al., 2020). This study further confirmed that mudstone, dolomitic mudstone and argillaceous dolomite were deposited under different salinity conditions of the water columns, according to Sr/Ba ratios, gammacerane index and β-carotane index. Moreover, As shown in Fig. 8C and D, with the increase of Sr/Ba ratios, C values decrease and Sr/Cu ratios increase, which suggests that the changes in water column salinity are mainly controlled by paleoclimate conditions. Further analysis (Fig. 7D–F) showed that the correlation between TOC and paleosalinity parameter is very low, suggesting that the paleosalinity is not a key factor controlling the organic matter enrichment.

### 5.2.3. Redox conditions

The redox conditions greatly affect the preservation of OM in lacustrine systems, thereby affecting the enrichment of organic matter (Bechtel et al., 2012; Strobl et al., 2014; Hackley et al., 2016). Redox-sensitive elements (eg. U, Mo, V, Ni) and biomarker parameters (eg. Pr/Ph, $Pr/NC_{17}$, $Ph/NC_{18}$) are useful indicators to evaluate redox conditions of the water column (Peters and Moldowan, 1993; Jones and Manning, 1994; Sarki Yandoka et al., 2015; Algeo and Liu, 2020). Cross-plotting $U_{EF}$ vs. $Mo_{EF}$ (EF = enrichment factor; $TE_{EF} = (TE/Al)_{sample}/(TE/Al)_{PAAS}$), a method for redox assessment, was applied to reflect redox environments, where $Mo_{EF}$ and $U_{EF}$ <10 reflect suboxic conditions whereas greater values reflect anoxic and euxinic conditions (Algeo and Tribovillard, 2009; Tribovillard et al., 2012). As shown in Fig. 6C, the $U_{EF}$ and $Mo_{EF}$ of fine-grained mixed sedimentary rocks in $P_2l$ range from 0.83 to 4.16 (avg. 1.98) and 0.81 to 6.35 (avg. 2.63), indicating a stable and suboxic water column conditions. In addition, the δU values ($\delta U = 2U/(U + Th/3)$ and $V/(V + Ni)$ ratios can also reflect redox conditions. δU<1.0 and δU>1.0 correspond to aerobic and anoxic conditions, respectively (Steiner et al., 2001). V/(V + Ni) ratios ≤0.46, >0.46 to ≤0.60, >0.60 to ≤0.82, >0.82 correspond to oxic, dysoxic, suboxic to anoxic and euxinic conditions respectively (Jones and Manning, 1994). The δU values and V/(V + Ni) ratios of fine-grained mixed sedimentary rocks in $P_2l$ were 1.33–1.83 (avg. 1.61), 0.65 to 0.81 (avg. 0.73), respectively (Table 5), suggesting that mudstone, dolomitic mudstone and argillaceous dolomite were deposited under a suboxic to anoxic environment.

Among biomarkers, N-alkanes and isoprenoid alkanes are commonly used to reflect redox conditions. Pr/Ph ratios of <0.8 and >3.0 correspond to typical anoxic conditions and oxic conditions, respectively (ten Haven et al., 1987; Peters and Moldowan, 1993). The crossplot of $Pr/NC_{17}$ vs. $Ph/NC_{18}$ can also reflect the redox environment of the water column (Shanmugam, 1985; Sarki Yandoka et al., 2015). As shown in Fig. 6B, the Pr/Ph of the $P_2l$ mixed sedimentary rocks ranges from 0.75 to 1.36 (avg.1.04), reflecting a suboxic to anoxic water column. These results are also confirmed by the crossplot of $Pr/NC_{17}$ vs. $Ph/NC_{18}$

(Fig. 6D).

In conclusion, the analysis results of elemental and organic geochemical indicators reached the same conclusion. Mudstone, dolomitic mudstone and argillaceous dolomite are wholly deposited under a suboxic to anoxic water column, and the redox conditions of the water column present a minor variation. Further analysis (Fig. 7G–I) showed that the correlation between TOC and redox parameter is considerably low. However, the weak correlation between TOC and redox parameters does not mean that redox conditions exert no impact on the enrichment of organic matter in the study area. The reason is that during the deposition of the $P_2l$ fine-grained mixed rocks, the lake basin water was stratified with high salinity, which promoted the formation of a suboxic to anoxic bottom water environment, resulting in better preservation of organic matter in the whole deposition process. Therefore, this relatively reducing condition is also an important factor conducive to the organic matter enrichment of the source rocks in the study area.

### 5.3. Organic matter origin and primary productivity

#### 5.3.1. Organic matter origin

In lacustrine basins, organic matter origin can be divided into endogenous organic matter and exogenous organic matter, among which endogenous organic matter mainly comes from algae, fungi and plankton in lakes, while exogenous organic matter mainly comes from terrestrial higher plants (Volkman, 1986; Peters and Moldowan, 1993). The source of organic matter is usually determined by the primary productivity and paleoenvironment during the deposition of organic matter (Ercegovac and Kostić, 2006; Ding et al., 2017). At present, organic matter origin is usually analyzed based on some good proxies such as organic macerals and biomarkers parameters (Tyson, 1995; Frimmel et al., 2004; Strobl et al., 2014).

Maceral analysis revealed that the organic macerals of the $P_2l$ source rocks are mainly composed of alginite, especially lamalginite (Fig. 3A and B). Lamalginite is common in brackish lacustrine source rocks, and records the geological history of algal growth, bloom, death and burial, reflecting the seasonal turnover of lake water (Wittkop et al., 2009; Hakimi et al., 2016; Liu et al., 2017). The high content of alginite indicates that the algae have an important contribution to the input of organic matter. In addition, the proportion of terrigenous organic matter (sporinite, vitrinite and inertinite) of the $P_2l$ source rocks is not very high, indicating that terrigenous higher plants are not the principal source of organic matter.

The thermal evolution of $P_2l$ source rocks in the study area is in the low mature to mature stage. Therefore, the distribution characteristics of N-alkanes can reflect the type combination of organic matter input in source rocks and indicate the relative amount of terrestrial and aquatic organic matter (Brassell et al., 1978; Ding et al., 2017). The N-alkanes of the $P_2l$ source rocks present a distribution pattern of single peak and front (Fig. 4A), with a relatively high $NC_{21}^{-}/NC_{22}^{+}$ ratio (0.69–1.85, avg. 1.11) (Table 4), indicating that the organic matter in the source rocks is mainly composed of aquatic organisms, followed by terrestrial higher plants (Bechtel et al., 2007). Moreover, the cross-plot between $Pr/NC_{17}$ and $Ph/NC_{18}$ was accordant with the above-mentioned results (Fig. 6D).

The relative abundance of $C_{27}$, $C_{28}$ and $C_{29}$ regular steranes is often used to reflect the source of organic matter (Seifert and Moldowan, 1978; Huang and Meinschein, 1979). In general, $C_{27}$ regular steranes are mainly derived from aquatic organisms such as zooplankton and algae (Mackenzie et al., 1982). $C_{28}$ regular steranes indicate specific phytoplankton types, such as diatoms and cyanobacteria containing chlorophyll-c (Knoll et al., 2007). This study suggests that the $C_{28}$ regular steranes in $P_2l$ source rocks are mainly derived from cyanobacteria rather than diatoms. Firstly, fossil remains show that diatoms originated in the Jurassic or Cretaceous, with a large time interval from the Permian Lucaogou Formation (Grantham and Wakefield, 1988). Secondly, previous studies have confirmed that modern cyanobacteria grown in glucose petri dishes can produce large amounts of ergosterol (1033.3 μg/g), which is a bioprecursor of $C_{28}$ regular steranes (Fagundes et al., 2019). Thirdly, studies on modern cyanobacteria have shown that the growth of cyanobacteria produces a high concentration of extracellular polymers (EPS), which appear as wavy anastomosing lamalginite in organic macerals (Fig. 3B) (Wingender et al., 1999; Hu, 2011). In addition, Liu et al. (2022) confirmed that the $C_{28}$ regular steranes in the $P_2l$ source rocks were derived from cyanobacteria based on the morphological characteristics of algae in the organic maceral and the isotopic composition of source rock kerogen.

$C_{29}$ regular steranes are usually derived from terrestrial higher plants (Volkman, 1986; Hao et al., 2011). In recent years, it has been reported that $C_{29}$ regular steranes can also be derived from some microalgae, such as green algae (Volkman et al., 1998; Ding et al., 2019). This study suggests that the abundant $C_{29}$ regular steranes in the $P_2l$ source rocks are mainly derived from green algae rather than terrestrial higher plants. Firstly, if the abundant $C_{29}$ regular steranes in the $P_2l$ source rocks were mainly derived from terrigenous higher plants, it is inconsistent with the I-$II_1$ organic matter type of the $P_2l$ source rocks according to the pyrolysis parameters (Fig. 2B). Secondly, the low abundance of long chain N-alkanes ($NC_{27\text{-}31}$) and the low content of terrigenous OM in organic macerals also indicate the low contribution of terrigenous organic matter (Fig. 4A and B; Table 2). Thirdly, $C_{29}$ regular steranes were abundant in the Ordovician source rocks of some basins in the USA, when green algae and dinoflagellates were widely distributed and there were no higher plants (Ryder et al., 1998). During the Permian, green algae were abundant and dinoflagellates relatively rare (Grantham and Wakefield, 1988), when the $P_2l$ source rocks were deposited with abundant $C_{29}$ regular steranes, similar to the Ordovician case above. In addition, previous studies based on organic petrography, molecular geochemistry and element geochemistry have also confirmed that $C_{29}$ regular steranes in the $P_2l$ are derived from salt-tolerant green algae (Liu et al., 2022; Zhi et al., 2023). Therefore, it can be inferred that abundant $C_{29}$ regular sterane in the $P_2l$ source rocks is a sign of the source of halotolerant green algae (Fu et al., 1990; Xia et al., 2021).

Fig. 9A–C demonstrates a significant correlation between the composition of regular steranes and the gammacerane index, indicating that the salinity of the water column is an important factor affecting the organic matter composition of the source in the lake basin. The salinity of the lake basin water column was significantly affected by paleoclimate (Fig. 8C and D). During arid paleoclimate conditions, evaporation could increase the salinity of the water column, resulting in a decrease in the proportion of freshwater algae (mainly bioprecursors of $C_{27}$ regular steranes) (Fig. 9A), and an increase in the proportion of halotolerant cyanobacteria (mainly bioprecursors of $C_{28}$ regular steranes) and halotolerant green algae (mainly bioprecursors of $C_{29}$ regular steranes) in endogenous organic matter (Fig. 9B and C). As shown in Fig. 9B, with the increase of gammacerane index, the abundance of $C_{28}$ regular steroids first increased and then decreased, mainly because cyanobacteria (which mainly provide bioprecursors of $C_{28}$ regular steranes) are slightly halotolerant organisms (Warren, 2016). As a result, the development of cyanobacteria in the high-salinity water column will be limited due to cell membrane damage and reduced enzyme activity (Singh et al., 2022). In addition, the arid paleoclimate conditions led to an increase in the salinity of the lake water column, which was conducive to the formation of dolomite and promoted the deposition of dolomitic mudstone and argillaceous dolomite. This is the primary reason why the abundance of $C_{27}$ regular steranes (indicating freshwater algae) in dolomitic mudstone and argillaceous dolostone is lower than that in mudstone, and the abundance of $C_{28}$ and $C_{29}$ regular steranes (indicating halotolerant cyanobacteria and green algae) is higher than that in mudstone (Fig. 10A–C). Therefore, the paleoclimate, by enhancing the intensity of evaporation and the salinity of the water column, resulted in significant differences in the proportions of algae species (freshwater algae, halotolerant cyanobacteria and green algae) in mudstone, dolomitic mudstone and argillaceous dolostone.

Further analysis (Fig. 10A–C) showed that the correlation between

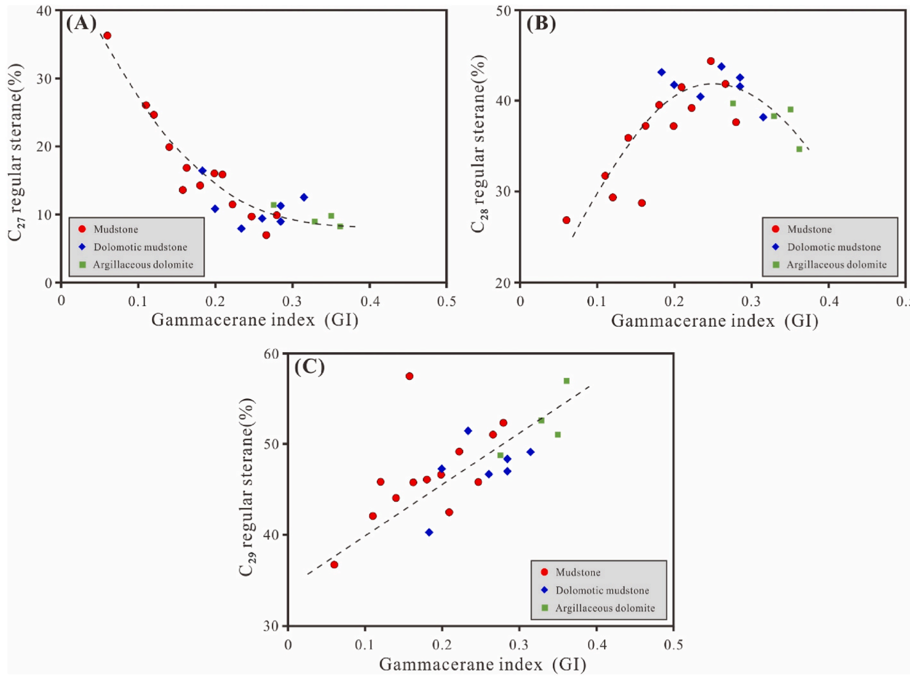


**Fig. 9.** Crossplots of regular steranes ($C_{27}$–$C_{29}$) versus gammacerane index of source rock samples from the $P_2l$ in Jimsar Sag.

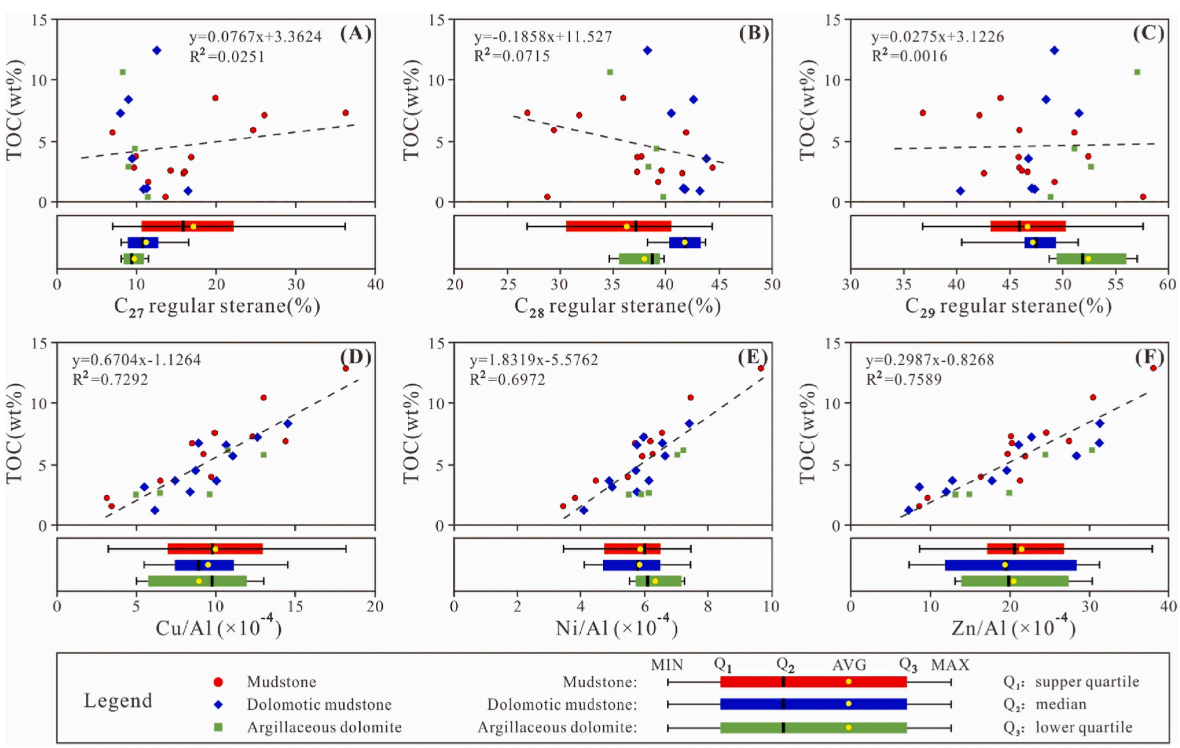


**Fig. 10.** The correlation between TOC and organic matter origin parameters (A–C: $C_{27}$, $C_{28}$, $C_{29}$ regular sterane), primary productivity parameters (D–F: Cu/Al, Ni/Al, Zn/Al) of source rock samples from the $P_2l$ in Jimsar Sag.

TOC and the proportion of $C_{27}$, $C_{28}$ and $C_{29}$ regular steranes in regular steranes are considerably low, indicating that the change of algae species (freshwater algae, halotolerant cyanobacteria and green algae) is not the main factor affecting the enrichment of organic matter. However, a positive relationship between TOC and alginate/terrestrial OM (Fig. 11A), indicating that the increasing proportion of algal organic matter has a significant contribution to the improvement of the abundance of organic matter in the source rocks, thus the increasing contribution of algal organic matter relative to the terrigenous organic matter has a favorable influence on the enrichment of organic matter.

### *5.3.2. Primary productivity*

Some trace elements in sediments can reflect primary productivity, such as Cu, Ni and Zn (Tribovillard et al., 2006; Schoepfer et al., 2015). Cu, Ni, and Zn exist mainly in organisms as nutrient elements, combine with organic matter to form organic complexes and precipitate at the

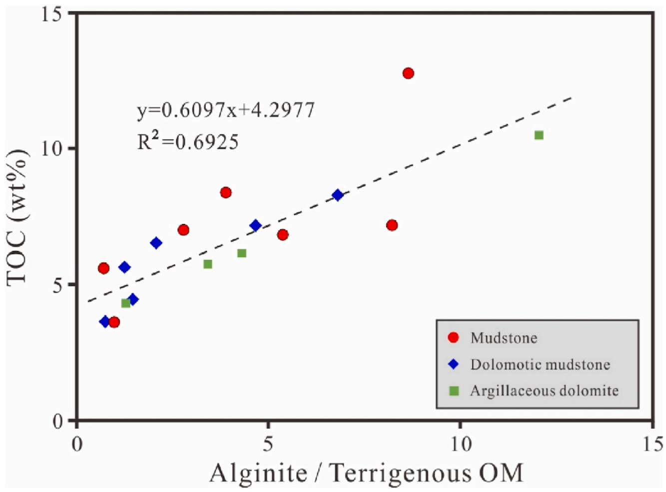


**Fig. 11.** Crossplots of TOC versus alginate/terrigenous OM in organic macerals of source rock samples from the $P_2l$ in Jimsar Sag.

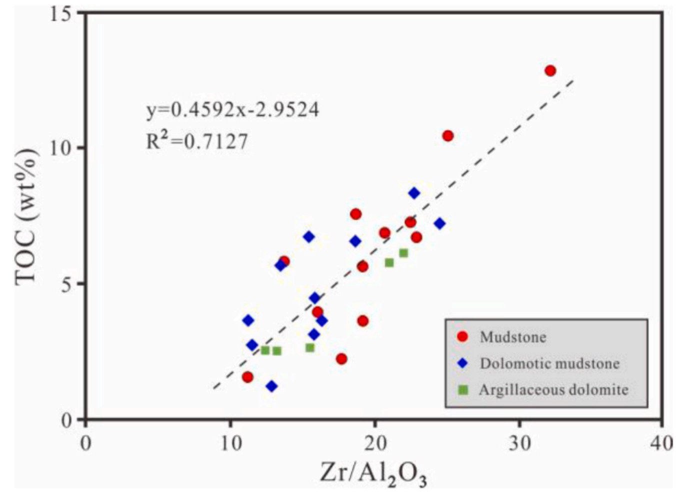


**Fig. 12.** Crossplots of TOC versus $Zr/Al_2O_3$ of source rock samples from the $P_2l$ in Jimsar Sag.

bottom of a lake or sea (Martin and Knauer, 1973; Boyle et al., 1977; Pruyers et al., 1991; Algeo and Maynard, 2004). Therefore, the accumulation of Cu, Ni and Zn in sediments is usually derived from the input of organic matter (Algeo and Maynard, 2004; Tribovillard et al., 2006; Schoepfer et al., 2015; Li et al., 2020). The elemental ratios Cu/Al, Ni/Al and Zn/Al, which eliminate the impact of terrigenous detrital, are effective indicators for evaluating primary productivity (Tribovillard et al., 2006; Schoepfer et al., 2015; Zeng et al., 2015). The higher ratios of Cu/Al, Ni/Al and Zn/Al, generally suggest a greater level of primary productivity (Tribovillard et al., 2006; Shen et al., 2014, 2015; Pan et al., 2020).

In comparison of Cu/Al (avg. 3.11), Ni/Al (avg. 5.48) and Zn/Al ratios (avg. 8.84) in the post-Archean Australian shale (Taylor and McLennan, 1985; McLennan, 1989), the source rocks of the $P_2l$ have higher Cu/Al ratios of 3.14–18.19 (avg. 9.58), Ni/Al ratios of 3.42–9.65 (avg. 5.93), Zn/Al ratios of 7.25–38.05 (avg. 20.49) are found to indicate a higher level of primary productivity. The geochemical parameters (Cu/Al, Ni/Al and Zn/Al ratios) reflecting the primary productivity of mudstone, dolomitic mudstone and argillaceous dolomite are not significantly different, while the above parameters fluctuate widely in source rocks of the same lithology type (Fig. 10D–F). Moreover, a positive correlation between TOC and primary productivity parameters (Cu/Al, Ni/Al and Zn/Al ratios) suggests that organic matter enrichment in the $P_2l$ source rocks is mainly controlled by primary productivity (Fig. 10D–F). The primary productivity of the $P_2l$ source rocks fluctuates greatly, which is influenced by the large-scale volcanic activity of Permian in Junggar Basin during the sedimentary period (Zhang et al., 2015; Hackley et al., 2016; Ding et al., 2017, 2020; Meng et al., 2022). Previous studies have confirmed the existence of tuffaceous detrital materials in the $P_2l$ source rocks based on thin section observations, indicating that volcanic activity influences the formation of source rocks (Ding et al., 2019; Su et al., 2019b; Zhang et al., 2019b; Meng et al., 2022). In addition, the $Zr/Al_2O_3$ ratio is considered to reflect the input of fine grained volcaniclastic particles and can be used as a relatively reliable geochemical indicator of volcanic ash input within fine-grained sediments (Suzuki et al., 1998; Pujol et al., 2006; Yang et al., 2022). The positive correlation between TOC and $Zr/Al_2O_3$ ratios (Fig. 12) indicates that the input of volcanic ash has an obvious promoting effect on the primary productivity of the $P_2l$ source rocks. When the volcanic activity is strong, Cu, Ni and Zn as nutrient elements carried by the volcanic ash fertilize the surface water, stimulate the flourishing of algae and enhance the primary productivity of lacustrine systems (Kurenkov, 1966; Erbacher et al., 1996; Delmelle et al., 2007; Langmann et al., 2010; Olgun et al., 2013; Li et al., 2021b; Pan et al., 2022). Conversely, during intermittent or weak periods of volcanic activity, algae growth is limited and primary productivity is relatively low.

### 5.4. Hydrothermal activity

XRD analysis results show that the $P_2l$ source rock has a high plagioclase content (6.0–61.0%, avg. 29.63%) and dolomite (1.0–67.0%, avg. 27.15%), respectively (Table 1), which are similar to the typical hydrothermal sedimentary rocks of the Lower Cretaceous in the Hari Sag, Yinyue Basin (Chen et al., 2018). Moreover, previous studies have shown that the $P_2l$ fine-grained sedimentary rocks were affected by hydrothermal activity, according to the petrographic observation, mineralogy and geochemical characteristics (Li et al., 2021a; Meng et al., 2022; Tao et al., 2022; Wu et al., 2022). Combined with the triangular plot of Ni–Co–Zn and Fe–Mn-(Cu + Co + Ni) × 10, most of the $P_2l$ source rock samples fall within the hydrothermal deposition fields, indicating that hydrothermal activity participated in the formation of source rocks through multi-stage physical and chemical processes (Fig. 13A and B).

Previous studies have confirmed that Li/Al and Cr/Zr ratios can indicate the intensity of hydrothermal activity (Marchig et al., 1982; Pisarskii et al., 1998; Pujol et al., 2006; Tao et al., 2022). The Li/Al ratios of the $P_2l$ mudstone, dolomitic mudstone and argillaceous dolomite in the study area are 5.62–21.23 (avg. 12.77), 10.84–36.80 (avg. 23.64) and 31.24–53.08 (avg. 40.89), respectively (Table 5). Cr/Zr ratios are 0.15–0.29 (avg. 0.22), 0.21–0.36 (avg. 0.28) and 0.29–0.42 (avg. 0.34), respectively (Table 5). The results indicate a gradual increase in the intensity of hydrothermal activity during the sedimentary period from mudstone, dolomitic mudstone to argillaceous dolomite. Naturally, frequent hydrothermal activity is typically indicative of heightened tectonic activity, and the occurrence of modern hydrothermal activity is always associated with tectonic activity (Gamo et al., 1996; Canales et al., 2007; Suo et al., 2017; Xu et al., 2023). Therefore, the contribution of hydrothermal activity caused by tectonic activity to the formation of mixed sedimentary rocks cannot be ignored. As shown in Fig. 14A and B, the content of Mg in the $P_2l$ source rock samples increased significantly with the enhancement of hydrothermal activity, the main reason is that the hydrothermal fluid was probably alkaline water, rich in $Mg^{2+}$, $Ca^{2+}$ and $CO_3^{2-}$ (Kenward et al., 2009). During the sedimentary period of the $P_2l$, varying degrees of tectonic activity resulted in hydrothermal activity of different intensities. The hydrothermal fluids carrying various metal ions (such as Mg, Fe, etc.) into the lake basin along the fault and fissure, which provided abundant sources of magnesium ions for the formation of dolomite. Further analysis (Fig. 14C and D) showed that

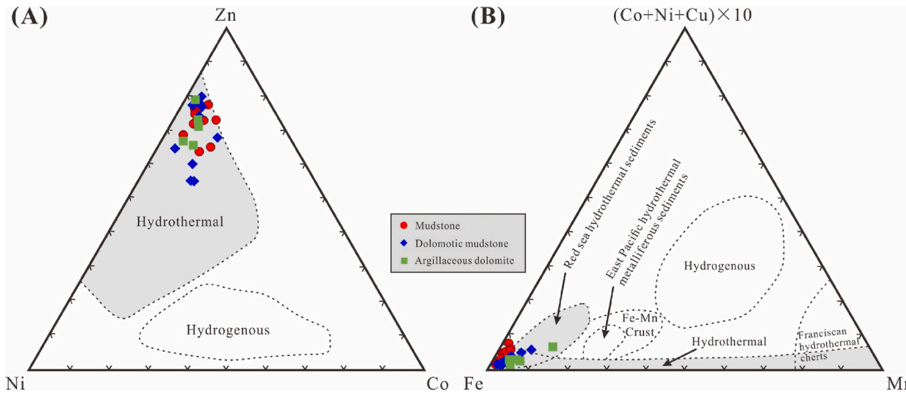


**Fig. 13.** (A) Triangular plot of Ni vs. Co vs. Zn after Choi and Hariya, 1992. (B) Triangular plot of Fe vs. Mn vs. (Cu + Co + Ni) × 10 after Crerar et al., 1982.

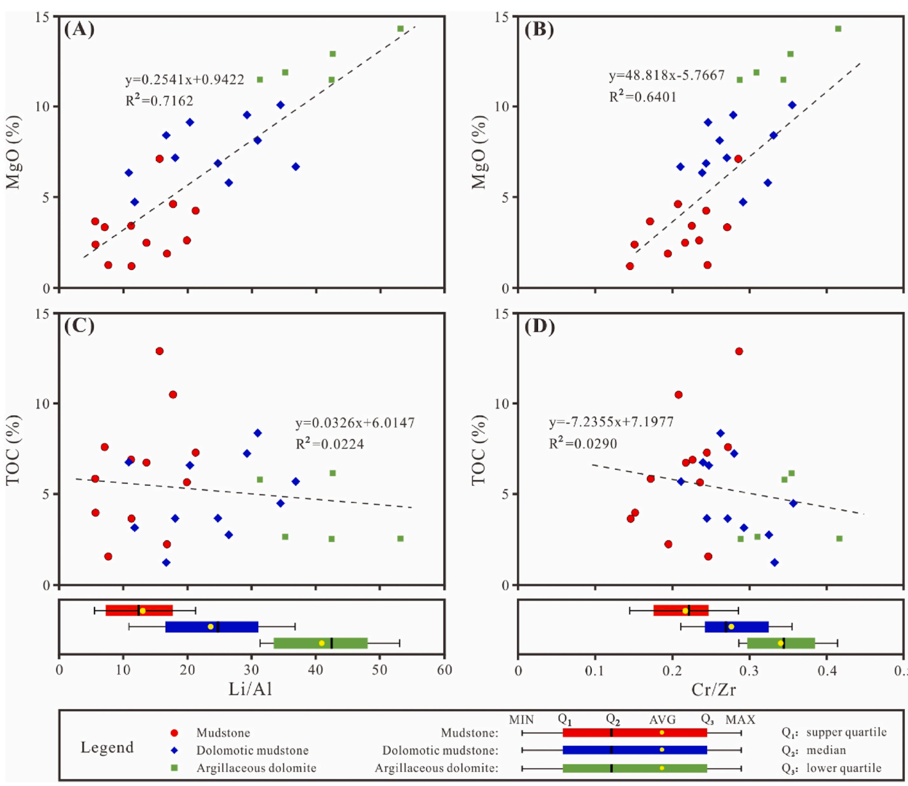


**Fig. 14.** Crossplots of MgO versus Li/Al (A); MgO versus Cr/Zr (B); TOC versus Li/Al (C); TOC versus Cr/Zr (D).

TOC had no significant correlation with the ratios of Li/Al and Cr/Zr, indicating that the intensity of hydrothermal activity was not the main factor affecting the organic matter enrichment in the $P_2l$ fine grained sedimentary rocks.

### *5.5. Formation mechanisms of organic-rich mixed sedimentary rocks*

The above analysis shows that the study area was in a relatively stable saline lacustrine sedimentary environment during the deposition of the $P_2l$ source rocks (Qiu et al., 2016; Tao et al., 2022), which created favorable conditions for the formation of organic-rich source rocks. During this period, the distribution area of felsic volcanic rocks in Shaqi and Santai uplifts, as sediment provenances, can provide some terrigenous clastic material for the study area. As mentioned above, there are obvious differences in the paleoenvironment during the deposition of mudstone, dolomitic mudstone and argillaceous dolomite. The paleoclimate of the mudstone deposition period is more humid than that of the dolomitic mudstone and argillaceous dolomite deposition period, and the evaporation is weak. Moreover, the hydrothermal activity is relatively weak. Therefore, the salinity and the $Mg^{2+}$ concentration of the water column in the lake basin are relatively low, which is not conducive to the precipitation of dolomite, resulting in a low content of dolomite in mudstone. Compared with mudstone, dolomitic mudstone and argillaceous dolomite were deposited under more arid paleoclimate conditions, and evaporation was further enhanced by arid paleoclimate. The hydrothermal fluids carried mantle source materials into the lake-bed, where a large amount of $Mg^{2+}$ input and arid-hot paleoclimate jointly promoted the mass precipitation of dolomite, leading to the formation of dolomitic mudstone and argillaceous dolomite. Therefore, the interbedded deposits of different types of mixed sedimentary rocks in the saline lacustrine basin of the $P_2l$ were formed as a result of the frequent changes in paleoclimate conditions and hydrothermal activity.

During the sedimentary period from mudstone, dolomitic mudstone to argillaceous dolomite, the paleoclimate conditions tended to be increasingly arid-hot, and the salinity of the water column gradually increased. The increased salinity of the water column exerts a significant effect on the change of algae species, which can increase the proportion of organic matter of halotolerant algae (cyanobacteria, green algae) relative to freshwater algae, resulting in a higher proportion of halotolerant algae organic matter in dolomitic mudstone and argillaceous dolomite than mudstone. As the salinity of the water column increased, the salt water environment further reduces the proportion of freshwater algae, resulting in a decrease in biodiversity, while the biomass does not decrease. Saline lakes are not the traditionally thought "biological deserts" (Warren, 2016). As the salinity of the water column increases, halotolerant algae (e.g., cyanobacteria, green algae, etc.) can replace freshwater algae and thrive in evaporative saltwater environments (Xia et al., 2021).

Volcanic activity played a key role in the enrichment of organic matter in source rocks. Although excessive input of volcanic materials can reduce the transparency of the water column, which is not conducive to the growth and development of organisms in the lake (Liu et al., 2021), the study area is located at the middle-distal distance from the volcanic eruption area (Mao et al., 2012; Meng et al., 2022), and the volcanic ash carried by the wind falls into the lake, bringing appropriate nutrients to the lake basin. During the strong period of volcanic activity, the input of volcanic ash provided abundant nutrients for algae to flourish and significantly promoted primary productivity, which is the key factor of organic matter enrichment in the mixed sedimentary rocks of the $P_2l$ in the study area. In addition, the high salinity in the saline lake basin resulted in stratification of the water column, coupled with oxygen consumption by massive algal blooms, enhanced the anoxia of the bottom water, which is suggested to be beneficial for the preservation of organic matter.

In conclusion, high primary productivity, strong preservation conditions, changes in paleoclimate and hydrothermal activity jointly promoted the formation of the $P_2l$ organic-rich mixed sedimentary rocks. The change of paleoclimate conditions and hydrothermal activity intensity mainly controls the formation of source rocks with different lithologies, the resulting change in salinity is the main factor contributing to the increased proportion of halotolerant algae in dolomitic mudstone and argillaceous dolomite. Additionally, the improvement in the primary productivity caused by volcanic activity is the key factor for the enrichment of organic matter in the mixed sedimentary rocks.

### *5.6. Implications*

Taking the Lucaogou Formation in Jimsal Sag as an example, this study revealed the differences in the formation mechanism of mixed sedimentary rocks (mudstone, dolomitic mudstone and argillaceous dolomite) in a saline lake basin, which has the following implications for subsequent research work: (1) The organic geochemical parameters, including the gammacerane index, β-carotane index and relative abundance of regular steranes of ($C_{27}$, $C_{28}$ and $C_{29}$), exhibit variations among mixed sedimentary rocks with different lithologies. According to these differences, the crude oil generated from different source rocks can be distinguished, which provides a basis for the oil-source correlation of the $P_2l$ in the Jimsar Sag. This is conducive to oil and gas exploration in the study area; (2) In both ancient and modern salt lakes, the gradual increase in water column salinity leads to a replacement of freshwater algae by halotolerant algae (e.g., cyanobacteria, green algae, etc.). Therefore, a comparison and analysis of the differences in hydrocarbon generation kinetics, evolution and models in the $P_2l$ source rocks derived mainly from freshwater algae and halotolerant algae can be conducted to further investigate whether changes in algae species lead to variations in hydrocarbon generation mechanism; (3) The lake water in saline lake basins usually exhibits high salinity and stable salinity stratification, resulting in anoxic conditions in the bottom water, which is conducive to the preservation of organic matter. Consequently, variations in primary productivity are likely the decisive factor behind differences in organic matter abundance among source rocks from various continental saline lacustrine basins.

## 6. Conclusions

(1) The mixed sedimentary strata of the $P_2l$ in Jimsar Sag are mainly composed of mudstone, dolomitic mudstone and argillaceous dolomite. The source rock with different lithologies has a high abundance of organic matter, and the type of OM is mainly type I and type $II_1$. All of them have high hydrocarbon generation potential and may form organic-rich source rocks.
(2) The periodic changes in paleoclimate and hydrothermal activity control the formation of different types of mixed sedimentary rocks. During the sedimentation period of the $P_2l$ in the study area, the salinity of the water column gradually increased as the paleoclimate gradually changed from warm-humid to air-hot and the enhancement of hydrothermal activity, resulting in the formation of mudstone, dolomitic mudstone and argillaceous dolomite successively.
(3) The organic matter of the mixed sedimentary rocks in the $P_2l$ is mainly derived from aquatic organisms such as algae, while the contribution of higher plants is minor. Paleoclimate and hydrothermal activity caused changes in the salinity of the water column in the lake basin. The increased salinity of the water column increased the proportion of halotolerant algae (cyanobacteria, green algae) relative to freshwater algae.
(4) During the sedimentary period of the $P_2l$, the continuous suboxic to anoxic bottom water environment was more conducive to the preservation of organic matter, and the increase of primary productivity caused by volcanic activity was the most critical factor to promote the enrichment of organic matter in the mixed sedimentary rocks.

## Credit author statement

The specific work of each author in this study was as follows: Wenren Zeng: Experiments, Software, Investigation, Writing - Original Draft. Zhihuan Zhang: Conceptualization, Methodology, Supervision. Boran Wang: Data curation, Review & Editing. Xuan Chen: Data curation, Review & Editing. Ruihui Zheng: Writing, Review & Editing. Guobin Fu: Experiments, Review & Editing. Ying Jin: Experiments, Review & Editing.

## Declaration of competing interest

The authors declare that they have no known competing financial interests or personal relationships that could have appeared to influence the work reported in this paper.

## Data availability

Data will be made available on request.

## Acknowledgements

This study is financially supported by the Cooperation Science and Technology Project (Grant No. KTGSZC 2020) of Tuha Oilfield Company of PetroChina Co. Ltd. and China University of Petroleum (Beijing).

## References

Algeo, T.J., Liu, J.S., 2020. A re-assessment of elemental proxies for paleoredox analysis. Chem. Geol. 540, 119549.
Algeo, T.J., Maynard, J.B., 2004. Trace-element behavior and redox facies in core shales of Upper Pennsylvanian Kansas-type cyclothems. Chem. Geol. 206 (3–4), 289–318.
Algeo, T.J., Tribovillard, N., 2009. Environmental analysis of paleoceanographic systems based on molybdenum-uranium covariation. Chem. Geol. 268 (3), 211–225.

Bai, Y.Y., Liu, Z.J., Sun, P.C., Liu, R., Hu, X.F., Zhao, H.Q., Xu, Y.B., 2015. Rare earth and major element geochemistry of Eocene fine-grained sediments in oil shale and coal-bearing layers of the Meihe Basin, northeast China. J. Asian Earth Sci. 97 (A), 89–101.
Bechtel, A., Jia, J.L., Strobl, S.A.I., Sachsenhofer, R.F., Liu, Z.J., Gratzer, R., Püttmann, W., 2012. Palaeoenvironmental conditions during deposition of the Upper cretaceous oil shale sequences in the Songliao Basin (NE China): implications from geochemical analysis. Org. Geochem. 46, 76–95.
Bechtel, A., Reischenbacher, D., Sachsenhofer, R.F., Gratzer, R., Lücke, A., Püttmann, W., 2007. Relations of petrographical and geochemical parameters in the middle Miocene Lavanttal lignite (Austria). Int. J. Coal Geol. 70, 325–349.
Boyle, E.A., Sclater, F.R., Edmond, J.M., 1977. The distribution of dissolved copper in the Pacific. Earth Planet Sci. Lett. 37, 38–54.
Brassell, S.C., Eglinton, G., Maxwell, J.R., Philp, R.P., 1978. Natural background of alkanes in the aquatic environment. Aqu. Poll. 1978, 69–86.
Brauchli, M., McKenzie, J.A., Strohmenger, C.J., Sadooni, F., Vasconcelos, C., Bontognali, T.R., 2015. The importance of microbial mats for dolomite formation in the Dohat Faishakh sabkha. Qatar Carb. Evap.. 31, 339–345.
Canales, J.P., Sohn, R.A., deMartin, B.J., 2007. Crustal structure of the Trans-Atlantic Geotraverse (TAG) segment (Mid-Atlantic Ridge, 26°10′N): implications for the nature of hydrothermal circulation and detachment faulting at slow spreading ridges. G-cubed 8 (8), Q08004.
Cao, H., Guo, W., Shan, X., Ma, L., Sun, P., 2015. Paleolimnological environments and organic accumulation of the Nenjiang Formation in the southeastern Songliao basin. China. Oil Shale 32 (1), 5–24.
Cao, Z., Liu, G.D., Kong, Y.H., Wang, C.Y., Niu, Z.C., Zhang, J.Y., Geng, C.B., Shan, X., Wei, Z.P., 2016. Lacustrine tight oil accumulation characteristics: permian Lucaogou Formation in Jimusaer sag, Junggar Basin. Int. J. Coal Geol. 153, 37–51.
Chen, Z., Ren, Z., Yu, C., Qi, K., Ren, W., Yang, Y., Ma, Q., 2018. Characteristics and Genetic Analysis of Hydrothermal Sediment of Lower Cretaceous in Hari Depression, Yin'e Basin. J. Earth Sci. 43 (6), 1941–1956.
Cheng, J., Meng, X., Zhang, E., Jiang, Q., Ni, Z., Ji, J., 2021. An early Holocene primary dolomite layer of abiotic origin in Lake Sayram, Central Asia. Geophys. Res. Lett. 48, 13.
Choi, J.H., Hariya, Y., 1992. Geochemistry and depositional environment of Mn oxide deposits in the Tokoro Belt, northeastern Hokkaido. Japan. Econ. Geol. 87 (5), 1265–1274.
Condie, K.C., Lee, D., Farmer, G.L., 2001. Tectonic setting and provenance of the Neoproterozoic Uinta Mountain and Big Cottonwood groups, northern Utah: constraints from geochemistry, Nd isotopes, and detrital modes. Sediment. Geol. 141, 443–464.
Connan, J., Cassou, A.M., 1980. Properties of gases and petroleum liquids derived from terrestrial kerogen at various maturation levels. Geochem. Cosmochim. Acta 44, 1–23.
Crerar, D.A., Namson, J., Chyi, M.S., Williams, L., Feigenson, M.D., 1982. Manganiferous cherts of the Franciscan assemblage; I, General geology, ancient and modern analogues, and implications for hydrothermal convection at oceanic spreading centers. Econ. Geol. 77 (3), 519–540.
Cullen, J.T., Field, M.P., Sherrell, R.M., 2001. Determination of trace elements in filtered suspended marine particulate material by sector field HR-ICP-MS. J. Anal. At. Spectrom. 16, 1307–1312.
Cullers, R.L., 1995. The controls on the major- and trace-element evolution of shales, siltstones and sandstones of Ordovician to Tertiary age in the wet mountains region, Colorado, USA. Chem. Geol. 123 (1), 107–131.
Custodio, E., 2002. Aquifer overexploitation: what does it mean? Hydrogeol. J. 10, 254–277.
Delmelle, P., Lambert, M., Dufrêne, Y., Gerin, P., Óskarsson, N., 2007. Gas/aerosol-ash interaction in volcanic plumes: new insights from surface analyses of fine ash particles. Earth Planet Sci. Lett. 259 (1–2), 159–170.
Ding, W.J., Hou, D.J., Jiang, L., Jiang, Y.H., Wu, P., 2020. High abundance of carotanes in the brackish-saline lacustrine sediments: a possible cyanobacteria source? Int. J. Coal Geol. 219, 103373.
Ding, X.J., Gao, C.H., Zha, M., Chen, H., Su, Y., 2017. Depositional environment and factors controlling β-carotane accumulation: a case study from the Jimsar Sag, Junggar Basin, northwestern China. Palaeogeogr. Palaeoclimatol. Palaeoecol. 485, 833–842.
Ding, X.J., Qu, J.X., Imin, A., Zha, M., Su, Y., Jiang, Z.F., Jiang, H., 2019. Organic matter origin and accumulation in tuffaceous shale of the lower Permian Lucaogou Formation, Jimsar Sag. J. Pet. Sci. Eng. 179, 696–706.
Ding, Y., Li, Z.W., Feng, F., Zhai, Z.H., Sun, W., Tang, C., Zhang, W., Zhang, C.J., Liu, S. G., 2013. Mixing of lacustrine siliciclastic-carbonate sediments and its significance for tight oil exploration in the Daanzhai Member, Ziliujing Formation, lower Jurassic, in Longgang area, central Sichuan Basin. Geol. Rev. 59 (2), 389–400.
Dong, G.Y., Chen, H.D., Li, J.W., Lin, L.B., Zhong, Y.J., Luo, J.X., Wang, F., Chen, A.Q., Li, J., 2009. The cambrian mixed sedimentation around bohai sea bay basin. Acta Geol. Sin. 83 (6), 800–811.
Dorsey, R.J., Kidwell, S.M., 1999. Mixed carbonate-siliciclastic sedimentation on a tectonically active margin, Example from the Pliocene of Baja California Sur, Mexico. Geol. 27 (10), 935–938.
Dunham, E.C., Fones, E.M., Fang, Y., Lindsay, M.R., Steuer, C., Fox, N., 2020. An ecological perspective on dolomite formation in Great Salt Lake, Utah. Front. Earth Sci. 8, 24.
Erbacher, J., Thurow, J., Littke, R., 1996. Evolution patterns of radiolaria and organic matter variations: a new approach to identify sea-level changes in mid-Cretaceous pelagic environments. Geology 24 (6), 499–502.
Ercegovac, M., Kostić, A., 2006. Organic facies and palynofacies: nomenclature, classification and applicability for petroleum source rock evaluation. Int. J. Coal Geol. 68 (1), 70–78.
Eugster, H.P., Hardie, L.A., 1978. Saline lakes. In: Lerman, A. (Ed.), Lakes: Chemistry, Geology, Physics. Springer, New York, pp. 237–293.
Fagundes, M.B., Falk, R.B., Facchi, M.M.X., Vendruscolo, R.G., Maroneze, M.M., Zepka, L.Q., Jacob-Lope, E., Wagner, R., 2019. Insights in cyanobacteria lipidomics: a sterols characterization from Phormidium autumnale biomass in heterotrophic cultivation. Food Res. Int. 119, 777–784.
Fang, S.H., Jia, C.Z., Song, Y., Xu, H.M., Liu, L.J., 2005. The tectonism during Yanshan Period in southern Junggar foreland basin and its implications for hydrocarbon accumulation. Earth Sci. Front. 12 (3), 67–76 (in Chinese with English abstract).
Fang, S.H., Song, Y., Xu, H.M., Fan, R.D., Liu, L.J., Xu, X.C., 2007. Relationship between tectonic evolution and Petroleum system formation. Pet. Geol. Exp. 29 (2), 149–161 (in Chinese with English abstract).
Feng, J.L., Cao, J., Hu, K., Peng, X.Q., Chen, Y., Wang, Y.F., Wang, M., 2013. Dissolution and its impacts on reservoir formation in moderately to deeply buried strata of mixed siliciclastic-carbonate sediments, northwestern Qaidam Basin, northwest China. Mar. Petrol. Geol. 39 (1), 124–137.
Frimmel, A., Oschmann, W., Schwark, L., 2004. Chemostratigraphy of the posidonia Black shale, SW Germany. Chem. Geol. 206 (3), 199–230.
Fu, J.M., Sheng, G.Y., Xu, J.Y., Eglinton, G., Gowar, A.P., Jia, R.F., Fan, S.F., Peng, P.A., 1990. Application of biological markers in the assessment of paleoenvironments of Chinese non – marine sediments. Org. Geochem. 16, 769–779.
Gamo, T., Nakayama, E., Shitashima, K., Isshiki, K., Obata, H., Okamura, K., Kanayama, S., Oomori, T., Koizumi, T., Matsumoto, S., 1996. Hydrothermal plumes at the Rodriguez triple junction, Indian ridge[J]. Earth Planet Sci. Lett. 142 (1–2), 261–270, 1996.
Gao, G., Yang, S.R., Ren, J.L., Zhang, W.W., Xiang, B.L., 2018. Geochemistry and depositional conditions of the carbonate-bearing lacustrine source rocks: a case study from the Early Permian Fengcheng Formation of Well FN7 in the northwestern Junggar Basin. J. Pet. Sci. Eng. 162, 407–418.
Gao, G., Zhang, W.W., Xiang, B.L., Liu, G.D., Ren, J.L., 2016. Geochemistry characteristics and hydrocarbon-generating potential of lacustrine source rock in Lucaogou Formation of the Jimusaer sag, Junggar Basin. J. Pet. Sci. Eng. 145, 168–182.
Grantham, P.J., Wakefield, L.L., 1988. Variations in the sterane carbon number distributions of marine source rock derived crude oils through geological time. Org. Geochem. 12, 61–73.
Hackley, P.C., Fishman, N., Wu, T., Baugher, G., 2016. Organic petrology and geochemistry of mudrocks from the lacustrine Lucaogou Formation, Santanghu Basin, northwest China: application to lake basin evolution. Int. J. Coal Geol. 168, 20–34.
Hakimi, M.H., Abdullah, W.H., Alqudah, M., Makeen, Y.M., Mustapha, K.A., 2016. Organic geochemical and petrographic characteristics of the oil shales in the Lajjun area, Central Jordan: origin of organic matter input and preservation conditions. Fuel 181, 34–45.
Hao, F., Zhou, X.H., Zhu, Y.M., Yang, Y.Y., 2011. Lacustrine source rock deposition in response to co–evolution of environments and organisms controlled by tectonic subsidence and climate, Bohai Bay Basin. China. Org. Geochem. 42, 323–339.
Hayashi, K.I., Fujisawa, H., Holland, H.D., Ohmoto, H., 1997. Geochemistry of approximately 1.9 Ga sedimentary rocks from northeastern Labrador, Canada. Geochem. Cosmochim. Acta 61, 4115–4137.
Hoffmann, L.J., Breitbarth, E., Ardelan, M., Duggen, S., Olgun, N., Hassellöv, M., Wängberg, S.Å., 2012. Influence of trace metal release from volcanic ash on growth of Thalassiosira pseudonana and Emiliania huxleyi. Mar. Chem. 132, 28–33.
Hopmans, E.C., Schouten, S., Rijpstra, W.I.C., Sinninghe Damsté, J.S., 2005. Identification of carotenals in sediments. Org. Geochem. 36, 485–495.
Hu, H.J., 2011. The Biology of Cyanobacteria. Science Press, Beijing.
Huang, W.Y., Meinschein, W.G., 1979. Sterols as ecological indicators. Geochem. Cosmochim. Acta 43, 739–745.
ICCP, 1998. The new vitrinite classification (ICCP System 1994). Fuel 77, 349–358.
ICCP, 2001. The new inertinite classification (ICCP System 1994). Fuel 80, 459–471.
Jin, Z.D., Zhang, E.L., 2002. Paleoclime implications of Rb/Sr ratios from lake sediments. Sci. Technol. Eng. 2 (3), 20–22 (in Chinese with English abstract).
Jones, B., Manning, D.A.C., 1994. Comparison of geochemical indices used for the interpretation of paleoredox conditions in. Chem. Geol. 111, 111–129.
Kenward, P.A., Goldstein, R.H., Gonzalez, L.A., Roberts, J.A., 2009. Precipitation of low-temperature dolomite from an anaerobic microbial consortium: the role of methanogenic Archaea. Geobiology 7, 556–565.
Knoll, A.H., Summons, R.E., Waldbauer, J.R., Zumberge, J.E., 2007. Chapter 8 - the geological succession of primary producers in the oceans. In: Falkowski, P.G., Knoll, A.H. (Eds.), Evolution of Primary Producers in the Sea. Academic Press, Burlington, pp. 133–163.
Kuang, L.C., Tang, Y., Lei, D.W., Chang, Q.S., Ouyang, M., Hou, L.H., Liu, D.G., 2012. Formation conditions and exploration potential of tight oil in the Permian saline lacustrine dolomitic rock, Junggar Basin, NW China. Petrol. Explor. Dev. 39 (6), 700–711 (in Chinese with English abstract).
Kurenkov, I.I., 1966. The influence of volcanic ash fall on biological processes in a lake. Limnol. Oceanogr. 11, 426–429.
Langmann, B., Zakšek, K., Hort, M., Duggen, S., 2010. Volcanic ash as fertiliser for the surface ocean. Atmos. Chem. Phys. 10, 3891–3899.
Lerman, A., 1978. Lakes: Chemistry, Geology. Physics. Springer, New York, pp. 237–289.
Li, H., Liu, Y., Yang, K., Liu, Y., Niu, Y., 2021a. Hydrothermal mineral assemblages of calcite and dolomite–analcime–pyrite in Permian lacustrine Lucaogou mudstones, eastern Junggar Basin. Northwest China. Mineral. Petrol. 115 (1), 63–85.

Li, L., Liu, Z.J., Jiang, L., George, S.C., 2021b. Organic petrology and geochemistry of Lower Cretaceous lacustrine sediments in the Chaoyang Basin (Liaoning Province, northeast China): influence of volcanic ash on algal productivity and oil shale formation. Int. J. Coal Geol. 233, 103653.

Li, Q., Wu, S.H., Xia, D.L., You, X.L., Zhang, H.M., Lu, H., 2020. Major and trace element geochemistry of the lacustrine organic-rich shales from the Upper Triassic Chang 7 Member in the southwestern Ordos Basin, China: implications for paleoenvironment and organic matter accumulation. Mar. Petrol. Geol. 111, 852–867.

Li, Q.Q., Xu, S., Hao, F., Shu, Z.G., Chen, F.L., Lu, Y.C., Wu, S.Q., Zhang, L., 2021c. Geochemical characteristics and organic matter accumulation of argillaceous dolomite in a saline lacustrine basin: a case study from the paleogene xingouzui formation, Jianghan Basin, China. Mar. Petrol. Geol. 128, 105041.

Li, W., Lu, S., Xue, H., Zhang, P., Hu, Y., 2015. Oil content in argillaceous dolomite from the Jianghan Basin, China: application of new grading evaluation criteria to study shale oil potential. Fuel 143, 424–429.

Lippmann, F., 1973. Sedimentary carbonate minerals. Earth Sci. Rev. 9, 388.

Liu, B., Bechtel, A., Gross, D., Fu, X., Li, X., Sachsenhofer, R.F., 2018. Middle Permian environmental changes and shale oil potential evidenced by high-resolution organic petrology, geochemistry and mineral composition of the sediments in the Santanghu Basin, Northwest China. Int. J. Coal Geol. 185, 119–137.

Liu, B., Bechtel, A., Sachsenhofer, R.F., Gross, D., Gratzer, R., Chen, X., 2017. Depositional environment of oil shale within the second member of permian Lucaogou Formation in the Santanghu Basin, northwest China. Int. J. Coal Geol. 175, 10–25.

Liu, C., Liu, K.Y., Wang, X.Q., Zhu, R.K., Wu, L.Y., Xu, X.Y., 2019. Chemo-sedimentary facies analysis of fine-grained sediment formations: an example from the Lucaogou Fm in the Jimusaer sag, Junggar Basin, NW China. Mar. Petrol. Geol. 110, 388–402.

Liu, G., Zhou, D., 2007. Application of microelements analysis in identifying sedimentary environment-taking Qianjiang Formation in the Jiang Han Basin as an example. Petrol. Geol. Exp. 29 (3), 307–311 (in Chinese with English abstract).

Liu, R., Zhang, K., Liu, Z.J., Yan, X., Yu, J.Q., 2021b. Oil shale mineralization and geological events in China. Acta Sedimentol. Sin. 39 (1), 10–28.

Liu, S.J., Gao, G., Jin, J., Gang, W.Z., Xiang, B.L., 2022. Source rock with high abundance of C28 regular sterane in typical brackish-saline lacustrine sediments: biogenic source, depositional environment and hydrocarbon generation potential in Junggar Basin, China. J. Pet. Sci. Eng. 208, 109670.

Ma, Y.Q., Fan, M., Lu, Y., Liu, H., Hao, Y., Xie, Z., Liu, Z.H., Peng, L., Du, X.B., Hu, H., 2016. Climate-driven paleolimnological change controls lacustrine mudstone depositional process and organic matter accumulation: constraints from lithofacies and geochemical studies in the Zhanhua Depression, eastern China. Int. J. Coal Geol. 167, 103–118.

Mackenzie, A.S., Brassell, S.C., Eglinton, G., Maxwell, J.R., 1982. Chemical fossils: the geological fate of steroids. Science 217, 491–504.

Mao, X., Li, J.H., Zhang, H.T., Wang, L., 2012. Study on the distribution and developmental environment of the Late Paleozoic volcanoes in Junggar Basin and its adjacent areas. Acta Petrol. Sin. 28 (7), 2381–2391 (in Chinese with English abstract).

Marchig, V., Gundlach, H., Möller, P., Schley, F., 1982. Some geochemical indicators for discrimination between diagenetic and hydrothermal metalliferous sediments. Mar. Geol. 50, 241–256.

Martin, J.H., Knauer, G.A., 1973. The elemental composition of plankton. Geochem. Cosmochim. Acta 37, 1639–1653.

Martins, L.L., Schulz, H.-M., Severiano Ribeiro, H.J.P., Nascimento, C.A.D., Souza, E.S.D., da Cruz, G.F., 2020. Organic geochemical signals of freshwater dynamics controlling salinity stratification in organic–rich shales in the lower Permian Irati Formation (Paran'a Basin, Brazil). Org. Geochem. 140, 103958.

McLennan, S.M., 1989. Rare earth elements in sedimentary rocks: influence of provenance and sedimentary processes. Rev. Mineral. Geochem. 21, 169–200.

McLennan, S.M., Hemming, S., McDaniel, D.K., Hanson, G.N., 1993. Geochemical approaches to sedimentation, provenance, and tectonics. Spec. Pap. Geol. Soc. Am. 284, 21–40.

Meng, Z.Y., Liu, Y.Q., Jiao, X., Ma, L.T., Zhou, D.W., Li, H., Cao, Q., Zhao, M.R., Yang, Y. Y., 2022. Petrological and organic geochemical characteristics of the permian Lucaogou Formation in the Jimsar sag, Junggar Basin, NW China: implications on the relationship between hydrocarbon accumulation and volcanic-hydrothermal activities. J. Pet. Sci. Eng. 210, 110078.

Moradi, A.V., Sarı, A., Akkaya, P., 2016. Geochemistry of the miocene oil shale (hançili formation) in the Çankırı-Çorum basin, Central Turkey: implications for paleoclimate conditions, source–area weathering, provenance and tectonic setting. Sediment. Geol. 341, 289–303.

Moldowan, J.M., Seifert, W.K., Gallegos, E.J., 1985. Relationship between petroleum composition and depositional environment of petroleum source rocks. AAPG Bull. 69 (8), 1255–1268.

Mount, J.F., 1984. Mixing of siliciclastic and carbonate sediments in shallow shelf environments. Geol. 12 (7), 432–435.

Murphy, S.M., McCormick, A., Eglinton, G., 1967. Perhydro–beta–Carotene in the green river shale. Science (New York, N.Y.) 157, 1040–1042.

Nishiyama, M., Sumikawa, Y., Guan, G., Marumoto, T., 2001. Relationship between microbial biomass and extractable organic carbon content in volcanic and non-volcanic ash soil. Appl. Soil Ecol. 17, 187.

Olgun, N., Duggen, S., Andronico, D., Kutterolf, S., Croot, P.L., Giammanco, S., Censi, P., Randazzo, L., 2013. Possible impacts of volcanic ash emissions of Mount Etna on the primary productivity in the oligotrophic Mediterranean Sea: results from nutrient-release experiments in seawater. Mar. Chem. 152, 32–42.

Palermo, D., Aigner, T., Geluk, M., Poeppelreiter, M., Pipping, K., 2008. Reservoir potential of a lacustrine mixed carbonate/siliciclastic gas reservoir: the lower Triassic Rogenstein in The Netherlands. J. Petrol. Geol. 31 (1), 61–96.

Pan, Y.S., Huang, Z.L., Guo, X.B., Wang, R., Lash, G.G., Fan, T.G., Liu, W.H., 2021. A re-assessment and calibration of redox thresholds in the permian Lucaogou Formation of Malang sag, Santanghu Basin, northwest China. Mar. Petrol. Geol. 135, 105406.

Pan, Y.S., Huang, Z.L., Li, T.J., Guo, X.B., Xu, X.F., Chen, X., 2020. Environmental response to volcanic activity and its effect on organic matter enrichment in the permian Lucaogou Formation of the Malang sag, Santanghu Basin, northwest China. Palaeogeogr. Palaeoclimatol. Palaeoecol. 560, 110024.

Pan, Y.S., Huang, Z.L., Li, T.J., Xu, X.F., Guo, X.B., Wang, R., Zheng, H.R., Zhang, W., 2022. Study on the origin and hydrocarbon generation potential of lacustrine organic-rich dolomite affected by volcanism: a case study of Lucaogou Formation in the Malang Sag, Santanghu Basin, Western China. Mar. Petrol. Geol. 141, 105699.

Peters, K.E., Cassa, M.R., 1994. Applied source rock geochemistry: chapter 5: Part II. In: Essential Elements.

Peters, K.E., Moldowan, C.C., 1993. The Biomarker Guide: Interpreting Molecular Fossils in Petroleum and Ancient Sediments. Prentic-Hall. Inc, Englewood Cliffs, New Jersey.

Peters, K.E., Walters, C.C., Moldowan, J.M., 2005. The Biomarker Guide. Biomarkers and Isotopes in Petroleum Exploration and Earth History. Cambridge University Press, New York.

Petrash, D.A., Bialik, O.M., Bontognali, T.R.R., Vasconcelos, C., Roberts, J.A., McKenzie, J.A., Konhauser, K.O., 2017. Microbially catalyzed dolomite formation: from near-surface to burial. Earth Sci. Rev. 171, 558–582.

Pickel, W., Kus, J., Flores, D., Kalaitzidis, S., Christanis, K., Cardott, B.J., Misz-Kennan, M., Rodrigues, S., Hentschel, A., Hamor-vido, M., Crosdale, P., Wagner, N., 2017. Classification of liptinite – ICCP system 1994. Int. J. Coal Geol. 169, 40–61.

Pisarskii, B.I., Konev, A.A., Levi, K.G., Delvaux, D., 1998. Carbon dioxide-bearing alkaline hydrotherms and strontium-bearing travertines in the songwe river valley (Tanzania). Geol. Geofiz. 39 (7), 941–948.

Poeppelreiter, M., Aigner, T., 2003. Unconventional pattern of reservoir facies distribution in epeiric successions: lessons from an outcrop analog (Lower Keuper, Germany). AAPG Bull. 87 (1), 39–70.

Pruyers, P.A., Delange, G.J., Middelburg, J.J., 1991. In: Geochemistry of eastern Mediterranean sediments:primary sediments composition and diagenetic alteration, 100, pp. 137–154.

Pujol, F., Berner, Z., Stüben, D., 2006. Palaeoenvironmental changes at the Frasnian/Famennian boundary in key European sections: chemostratigraphic constraints. Palaeogeogr. Palaeoclimatol. Palaeoecol. 240 (1–2), 120–145.

Qi, X.F., He, Y.S., Zhao, L., Jiang, J.C., 2013. Palaeoecological environment of permian Lucaogou Formation of Santanghu Basin in Xinjiang. Xinjing Pet. Geol. 34, 623–626 (in Chinese with English abstract).

Qian, Q., Gao, J., Klemd, R., He, G., Song, B., Liu, D., Xu, R., 2009. Early Paleozoic tectonic evolution of the Chinese South Tianshan Orogen: constraints from SHRIMP zircon U-Pb geochronology and geochemistry of basaltic and dioritic rocks from Xiate, NW China. Int. J. Earth Sci. 98, 551–569.

Qiu, X.W., Liu, C.Y., Wang, F.F., Deng, Y., Mao, G.Z., 2015. Trace and rare earth element geochemistry of the upper triassic mudstones in the southern ordos basin, central China. Geol. J. 50 (4), 399–413.

Qiu, Z., Tao, H.F., Zou, C.N., Ji, H.J., Zhou, S.X., 2016. Lithofacies and organic geochemistry of the middle permian Lucaogou Formation in the Jimusar sag of the Junggar Basin, NW China. J. Pet. Sci. Eng. 140, 97–107.

Qu, C.S., Qiu, L.W., Yang, Y.Q., Yu, K.H., Tang, L.L., Wan, M., 2019. Environmental response of the permian volcanism in Lucaogou Formation in Jimsar, Junggar Basin, northwest China. Seismol. Geol. 3, 789–802.

Rakocinski, M., Zaton, M., Marynowski, L., Gedl, P., Lehmann, J., 2018. Redox conditions, productivity, and volcanic input during deposition of uppermost Jurassic and Lower Cretaceous organic-rich siltstones in Spitsbergen, Norway. Cretac. Res. 89, 126–147.

Rohling, E.J., 2000. Paleosalinity: confidence limits and future applications. Mar. Geol. 163, 1–11.

Roser, B.P., Palmer, K., Nathan, S., Cooper, R.A., Tulloch, A.J., 1995. Whole-rock Analyses of Paleozoic Sedimentary Rocks from the Buller and Takaka Terranes. Institute of Geological and Nuclear Sciences report 95/14.

Ryder, R.T., Burruss, R.C., Hatch, J.R., 1998. Black shale source rocks and oil generation in the Cambrian and Ordovician of the central Appalachian Basin, USA. AAPG Bull. 82, 412–441.

Sadooni, F., Howari, F., El-Saiy, A., 2010. Microbial dolomites from carbonate-evaporite sediments of the coastal Sabkha of Abu Dhabi and their exploration implications. J. Petrol. Geol. 33, 289–298.

Sarki Yandoka, B.M., Abdullah, W.H., Abubakar, M.B., Hakimi, M.H., Adegoke, A.K., 2015. Geochemical characterisation of early cretaceous lacustrine sediments of Bima formation, Yola Sub-basin, northern Benue trough, NE Nigeria: organic matter input, preservation, paleoenvironment and palaeoclimatic conditions. Mar. Petrol. Geol. 61, 82–94.

Sawyer, E.W., 1986. The influence of source rock type, chemical weathering and sorting on the geochemistry of clastic sediments from the Quetico metasedimentary belt, Superior Province. Canda. Chem. Geol. 55, 77–95.

Scalan, E.S., Smith, J.E., 1970. An improved measure of the odd–even predominance in the normal alkanes of sediment extracts and petroleum. Geochem. Cosmochim. Acta 34, 611–620.

Schoepfer, S.D., Shen, J., Wei, H.Y., Tyson, R.V., Ingall, E., Algeo, T.J., 2015. Total organic carbon, organic phosphorus, and biogenic barium fluxes as proxies for paleo-marine productivity. Earth Sci. Rev. 149, 23–52.

Seifert, W.K., Moldowan, J.M., 1978. Applications of steranes, terpanes and monoaromatics to the maturation, migration and source of crude oils. Geochem. Cosmochim. Acta 42, 77–95.

Shanmugam, G., 1985. Significance of coniferous rain forests and related organic matter in generating commercial quantities of oil, Gippsland Basin, Australia. AAPG Bull. 69, 1241–1254.

Shen, J., Schoepfer, S.D., Feng, Q.L., Zhou, L., Yu, J.X., Song, H.Y., Wei, H.Y., Algeo, T.J., 2015. Marine productivity changes during the end-Permian crisis and Early Triassic recovery. Earth Sci. Rev. 149, 136–162.

Shen, J., Zhou, L., Feng, Q.L., Zhang, M.H., Lei, Y., Zhang, N., Yu, J.X., Gu, S.Z., 2014. Paleo-productivity evolution across the Permian-Triassic boundary and quantitative calculation of primary productivity of black rock series from the Dalong Formation. South China. Sci. China Earth Sci. 57, 1583–1594.

Singh, P., Fillat, M., Kumar, A., 2022. Cyanobacterial Lifestyle and its Applications in Biotechnology. Academic Press.

Sinninghe Damsté, J.S., Kenig, F., Koopmans, M.P., Köster, J., Schouten, S., Hayes, J.M., de Leeuw, J.W., 1995. Evidence for gammacerane as an indicator of water column stratification. Geochem. Cosmochim. Acta 59, 1895–1900.

Slaughter, M., Hill, R.J., 1991. The influence of organic matter in organogenic dolomitization. J. Sediment. Petrol. 61, 296–303.

Steiner, M., Wallis, E., Erdtmann, B.D., Zhao, Y.L., Yang, R.D., 2001. Submarine –hydrothermal exhalative ore layers in black shales from South China and associated fossils – insights into a lower Cambrian facies and bio-evolution. Palaeogeogr. Palaeoclimatol. Palaeoecol. 169, 165–191.

Strobl, S.A.I., Sachsenhofer, R.F., Bechtel, A., Gratzer, R., Gross, D., Bokhari, S.N.H., Liu, R., Liu, Z.J., Meng, Q.T., Sun, P.C., 2014. Depositional environment of oil shale within the Eocene Jijuntun Formation in the Fushun basin (NE China). Mar. Petrol. Geol. 56, 166–183.

Stumm, W., Morgan, J.J., 1981. Aquatic Chemistry. Wiley, New York.

Su, S.Y., Jiang, Z.X., Shan, X.L., Ning, C.X., Zhu, Y.F., Wang, X.Y., Li, Z., Zhu, R.F., 2019a. Effect of lithofacies on shale reservoir and hydrocarbon bearing capacity in the Shahejie Formation, Zhanhua Sag, eastern China. J. Pet. Sci. Eng. 174, 1303–1308.

Su, Y., Zha, M., Ding, X.J., Qu, J.X., Gao, C.H., Jin, J.H., Iglauer, S., 2019b. Petrographic, palynologic and geochemical characteristics of source rocks of the Permian Lucaogou formation in Jimsar Sag, Junggar Basin, NW China: origin of organic matter input and depositional environments. J. Pet. Sci. Eng. 183, 106364.

Sun, F.N., Hu, W.X., Cao, J., Wang, X.L., Zhang, Z.R., Ramezani, J., Shen, S.Z., 2022. Sustained and intensified lacustrine methane cycling during Early Permian climate warming. Nat. Commun. 13, 4856.

Sun, F.N., Hu, W.X., Wang, X.L., Cao, J., Fu, B., Wu, H.G., Yang, S.C., 2021. Methanogen microfossils and methanogenesis in Permian lake deposits. Geology 49, 13–18.

Suo, Y., Li, S., Li, X., Zhang, Z., Ding, D., 2017. The potential hydrothermal systems unexplored in the Southwest Indian Ocean. Mar. Geophys. Res. 38 (1–2), 61–70.

Suzuki, N., Ishida, K., Shinomiya, Y., Ishiga, H., 1998. High productivity in the earliest Triassic ocean: black shales, Southwest Japan. Palaeogeogr. Palaeoclimatol. Palaeoecol. 141, 53–65.

Tanaka, K., Akagawa, F., Yamamoto, K., Tani, Y., Kawabe, I., Kawai, T., 2007. Rare earth element geochemistry of Lake Baikal sediment: its implication for geochemical response to climate change during the Last Glacial/Interglacial transition. Quat. Sci. Rev. 26 (9), 1362–1368.

Tang, L., Song, Y., Pang, X.Q., Jiang, Z.X., Guo, Y.C., Zhang, H.A., Pan, Z.H., Jiang, H., 2019. Effects of paleo sedimentary environment in saline lacustrine basin on organic matter accumulation and preservation: a case study from the Dongpu Depression, Bohai Bay Basin, China. J. Pet. Sci. Eng. 185 (3), 106669.

Tao, S., Shan, Y.S., Tang, D.Z., Xu, H., Li, S., Cui, Y., 2016. Mineralogy, major and trace element geochemistry of Shichanggou oil shales, Jimusaer, Southern Junggar Basin, China: implications for provenance, palaeoenvironment and tectonic setting. J. Pet. Sci. Eng. 146, 432–445.

Tao, S., Xu, Y., Tang, D., Xu, H., Li, S., Chen, S., Liu, W., Cui, Y., Gou, M., 2017. Geochemistry of the Shitoumei oil shale in the Santanghu Basin, Northwest China: implications for paleoclimate conditions, weathering, provenance and tectonic setting. Int. J. Coal Geol. 184, 42–56.

Tao, H.F., Qiu, Z., Qu, Y.Q., Liu, J., Qin, Z., Xie, Z.B., Qiu, J.L., Liu, B., 2022. Geochemistry of middle permian lacustrine shales in the Jimusar sag, Junggar Basin, NW China: implications for hydrothermal activity and organic matter enrichment. J. Asian Earth Sci. 232, 105267.

Taylor, S.R., McLennan, S.M., 1985. The Continental Crust: its Composition and Evolution. Blackwell, Oxford.

ten Haven, H.L., Leeuw, J.W., Rullkötter, J., Sinninghe Damsté, J.S., 1987. Restricted utility of the pristane/phytane ratio as a palaeoenvironmental indicator. Nature 330, 641–643.

Tribovillard, N., Algeo, T.J., Lyons, T., Riboulleau, A., 2006. Trace metals as paleoredox and paleoproductivity proxies: an update. Chem. Geol. 232, 12–32.

Tribovillard, N., Algeo, T.J., Baudin, F., Riboulleau, A., 2012. Analysis of marine environmental conditions based on molybdenum–uranium covariation—applications to Mesozoic paleoceanography. Chem. Geol. 324–325, 46–58.

Turgeon, S., Brumsack, H.J., 2006. Anoxic vs dysoxic events reflected in sediment geochemistry during the Cenomanian–Turonian boundary event (Cretaceous) in the Umbria–Marche Basin of central Italy. Chem. Geol. 234, 321–339.

Tyson, R.V., 1995. Sedimentary Organic Matter: Organic Facies and Palynofacies. Chapman & Hall, London, p. 615.

Volkman, J.K., 1986. A review of sterol markers for marine and terrigenous organic matter. Org. Geochem. 9, 83–99.

Volkman, J.K., Barrett, S.M., Blackburn, S.I., Mansour, M.P., Gelin, F., 1998. Microalgal biomarkers: a review of recent research developments. Org. Geochem. 29, 1163–1179.

Wang, Y.C., Cao, J., Tao, K.Y., Xiao, W.Y., Xiang, B.L., Li, E.T., Pan, C.C., 2021. Absence of β -carotane as proxies of hydrothermal activity in brackish lacustrine sediments. Palaeogeogr. Palaeoclimatol. Palaeoecol. 587, 110801.

Warren, J.K., 2016. Evaporites. Springer, Berlin.

Warthmann, R., Van, L.Y., Vasconcelos, C., McKenzie, J.A., Karpoff, A.M., 2000. Bacterially induced dolomite precipitation in anoxic culture experiments. Geology 28, 1091–1094.

Wei, W., Algeo, T.J., Lu, Y., Lu, Y., Liu, H., Zhang, S., Peng, L., Zhang, J., Chen, L., 2018. Identifying marine incursions into the Paleogene Bohai Bay Basin lake system in northeastern China. Int. J. Coal Geol. 200, 1–17.

Wingender, J., Neu, T.R., Flemming, H.-C., 1999. What are bacterial extracellular polymeric substances? In: Wingender, J., Neu, T.R., Flemming, H.-C. (Eds.), Microbial Extracellular Polymeric Substances: Characterization, Structure and Function. Springer-Verlag, Berlin Heidelberg, pp. 1–19.

Wittkop, C.A., Teranes, J.L., Dean, W.E., Guilderson, T.P., 2009. A lacustrine carbonate record of Holocene seasonality and climate. Geol. 37, 695–698.

Wright, D.T., 1997. An organogenic origin for widespread dolomite in the cambrian Eilean Dubh formation, northwestern Scotland. J. Sediment. Res. 67, 54–64.

Wu, A.B., Cao, J., Zhang, J.K., Wu, T., Wang, Y.C., 2022. Origin of microbial–hydrothermal bedded dolomites in the Permian Lucaogou Formation lacustrine shales, Junggar Basin, NW China. Sediment. Geol. 440, 106260.

Wu, F.Y., Yang, Y.H., Mitchell, R.H., Bellatreccia, F., Li, Q.L., Zhao, Z.F., 2010. In situ U–Pb and Nd–Hf–(Sr) isotopic investigations of zirconolite and calzirtite. Chem. Geol. 277, 178–195.

Wu, H., Hu, W., Cao, J., Wang, X., Wang, X., Liao, Z., 2016. A unique lacustrine mixed dolomitic-clastic sequence for tight oil reservoir within the middle Permian Lucaogou Formation of the Junggar Basin, NW China: reservoir characteristics and origin. Mar. Petrol. Geol. 76, 115–132.

Wu, Z.Y., Zhao, X.Z., Wang, E.Z., Pu, X.G., Lash, G., Han, W.Z., Zhang, W., Feng, Y., 2021. Sedimentary environment and organic enrichment mechanisms of lacustrine shale: a case study of the paleogene Shahejie Formation, Qikou sag, bohai Bay Basin. Palaeogeogr. Palaeoclimatol. Palaeoecol. 573, 110404.

Xia, L.W., Cao, J., Hu, W.X., Zhi, D.M., Tang, Y., Li, E.T., He, W.J., 2021. Coupling of paleoenvironment and biogeochemistry of deep-time alkaline lakes: a lipid biomarker perspective. Earth Sci. Rev. 213, 103499.

Xiao, W.J., Windley, B.F., Huang, B.C., Han, C.M., Yuan, C., Chen, H.L., Sun, M., Sun, S., Li, J.L., 2009. End-Permian to mid-Triassic termination of the accretionary processes of the southern Altaids: implications for the geodynamic evolution,Phanerozoic continental growth and metallogeny of Central Asia. Int. J. Earth Sci. 98 (6), 1189–1217.

Xie, X.M., Volkman, J.K., Qin, J.Z., Borjigin, T., Bian, L.Z., Zhen, L.J., 2014. Petrology and hydrocarbon potential of microalgal and macroalgal dominated oil shales from the Eocene Huadian Formation, NE China. Int. J. Coal Geol. 124, 36–47.

Xu, X., Liao, S.L., Tao, C.H., Liu, L.S., 2023. Quantifying the influence of magmatism and tectonism on ultraslow-spreading-ridge hydrothermal activity: evidence from the Southwest Indian Ridge. Geosci. Front. 14, 101584.

Yang, S.C., Hu, W.X., Fan, J.X., Deng, Y.Y., 2022. New geochemical identification fingerprints of volcanism during the Ordovician-Silurian transition and its implications for biological and environmental evolution. Earth Sci. Rev. 228, 104016.

Zeng, S.Q., Wang, J., Fu, X.G., Chen, W.B., Feng, X.L., Wang, D., Song, C.Y., Wang, Z.W., 2015. Geochemical characteristics, redox conditions, and organic matter accumulation of marine oil shale from the changliang mountain area, northern tibet, China. Mar. Petrol. Geol. 64, 203–221.

Zhang, J.Y., Liu, G.D., Cao, Z., Tao, S.Z., Felix, M., Kong, Y.H., Zhang, Y.Y., 2019a. Characteristics and formation mechanism of multi-source mixed sedimentary rocks in a saline lake, a case study of the Permian Lucaogou Formation in the Jimusaer Sag, northwest China. Mar. Petrol. Geol. 102, 704–724.

Zhang, K., Liu, R., Liu, Z.J., Li, B.L., Han, J.B., Zhao, K.A., 2020. Influence of volcanic and hydrothermal activity on organic matter enrichment in the Upper Triassic Yanchang Formation, southern Ordos Basin, Central China. Mar. Petrol. Geol. 112, 104059.

Zhang, S., Liu, Y.Q., Jiao, X., Zhou, D.W., Zhang, X., Lu, S.T., Zhou, N.C., 2018a. Sedimentary environment and formation mechanisim of dolomitic rocks in the middle permian Lucaogou Formation, Jimusar depression, Junggar Basin. J. Palaeogeogr. 20 (1), 33–48 (in Chinese with English abstract).

Zhang, S., Wu, T., Zhang, S., Cao, C., Ma, W., Shi, J., Sun, G., 2015. Organofacies and paleoenvironment of lower carboniferous mudstones (Dishuiquan formation) in eastern Junggar, NW China. Int. J. Coal Geol. 150, 7–18.

Zhang, S.H., Liu, C.Y., Liang, H., Wang, J.Q., Bai, J.K., Yang, M.H., Liu, G.H., Huang, H. X., Guan, Y.Z., 2018b. Paleoenvironmental conditions, organic matter accumulation, and unconventional hydrocarbon potential for the Permian Lucaogou Formation organic-rich rocks in Santanghu Basin, NW China. Int. J. Coal Geol. 185, 44–60.

Zhang, S.M., Cao, Y.C., Liu, K.Y., Jahren, J., Xi, K.L., Zhu, R.K., Yang, T., Cao, X., Wang, W., 2019b. Characterization of lacustrine mixed fine-grained sedimentary rocks using coupled chemostratigraphic-petrographic analysis: a case study from a tight oil reservoir in the Jimusar Sag, Junggar Basin. Mar. Petrol. Geol. 99, 453–472.

Zhang, Y., Sun, Y., Chen, J., 2020. Stable carbon isotope evidence for the origin of C28 steranes in lacustrine source rocks from the Qikou Sag, Bohai Bay Basin, Eastern China. Org. Geochem. 145, 104028.

Zhao, Z.Y., Zhao, J.H., Wang, H.J., Liao, J.D., Liu, C.M., 2007. Distribution characteristics and applications of trace elements in Junggar basin. Nat. Gas Explorat. Dev. 30, 30–33 (in Chinese with English abstract).

Zhi, D.M., Xiang, B.L., Zhou, N., Li, E.T., Zhang, C.J., Wang, Y.C., Cao, J., 2023. Contrasting shale oil accumulation in the upper and lower sweet spots of the lacustrine Permian Lucaogou Formation, Junggar Basin, China. Mar. Petrol. Geol. 150, 106178.